

Tsunami sedimentary deposits of Crete records climate during the ‘Minoan Warming Period’ (≈ 3350 yr BP)

The Holocene
2018, Vol. 28(6) 914–929
© The Author(s) 2018
Reprints and permissions:
sagepub.co.uk/journalsPermissions.nav
DOI: 10.1177/0959683617752840
journals.sagepub.com/home/hol
 SAGE

Christophe Lécuyer,^{1,2} François Atrops,¹ Romain Amiot,¹
Delphine Angst,¹ Valérie Daux,³ Jean-Pierre Flandrois,⁴
François Fourel,¹ Kevin Rey,¹ Aurélien Royer,¹ Magali Seris,¹
Alexandra Touzeau¹ and Denis–Didier Rousseau^{5,6}

Abstract

Earthquakes or explosive eruptions generate tsunamis, which are at the origin of thick and chaotic coastal sediments. These commonly fossiliferous deposits are formed instantaneously at the historical or geological timescale and therefore have the potential to provide snapshot records of past climates. In Crete, near the city of Palaikastro, crops out a 1- to 9-m-thick sedimentary layer deposited by a huge tsunami that has been previously estimated to be about 9 m high. The presence of volcanic ash, the geometry, the archeological and faunal contents of the sedimentary deposit along with radiocarbon dating converge for interpreting this tsunamite as coeval with the Minoan Santorini (Thera) eruption ≈ 3350 yr BP. During its drawback, the tsunami deposited rocky blocks and a muddy matrix containing mollusc shells dredged from the seabed as well as cattle skeletal remains and various artifacts belonging to the contemporaneous Minoan civilization. While the oxygen isotope compositions of terrestrial vertebrate bone remains most likely resulted from diagenetic alteration, those of a bovid tooth revealed that air temperatures during MM3 and LM1 periods were about 4°C higher than nowadays. Oxygen isotope measurements of marine mollusc shells also revealed that sea surface temperatures were higher by about 2°C. Those results compare with the 2.5°C temperature difference already estimated according to both $\delta^2\text{H}$ and $\delta^{18}\text{O}$ values of Greenland ice cores. Incremental sampling of marine gastropods and bovid teeth suggests that the seasonal amplitude was similar to that prevailing during the second half of the 20th century.

Keywords

climate, Crete, ‘Minoan Period’, seasonality, stable isotopes, Thera, tsunamite

Received 19 May 2017; revised manuscript accepted 11 November 2017

Introduction

Natural archives that record climatic parameters from a given area are theoretically quite numerous. In the marine environment, those archives are sedimentary deposits, more or less continuous over time, to which access is gained through international programs of oceanic drilling either in shallow or deep water. In the terrestrial environment, lacustrine deposits, speleothems, pollen assemblages, and remains of small and large mammals that were preserved in karstic deposits are available (e.g. Goring et al., 2009; Lécuyer et al., 2016; Legendre, 1986; McDermott, 2004). Conventional and stable isotope dendrochronology, both based on the study of the width wood rings and their H, C, and O isotope compositions, are also used for the quantification of air temperatures, amount of precipitation, and nebulosity (McCarroll and Loader, 2004; Speer, 2010). Nevertheless, tree ring methods are all based on a set of samples that must be representative of the original population of trees, which is rarely possible for past periods (e.g. Esper et al., 2016). A major challenge is to obtain climatic data both in the marine and terrestrial domains for a specific period of time. Stable carbon and oxygen isotope compositions of biogenic skeletal remains of terrestrial (vertebrate teeth and bones) and marine (zooplankton, corals, molluscs, fish) origin that have been accumulated in the sedimentary deposits formed by tsunami waves may therefore provide access to several key

variables of the climate such as the mean air and seawater temperatures, and their seasonal variations. Tsunami deposits, also called tsunamites, instantly formed at the geological or even historical timescale, trapping elements of the civilization (construction elements, art works, domestic artifacts) as well as living organisms (molluscs, fish, small mammals, cattle, human beings), which have perished in the devastating tsunami.

¹Laboratoire de Géologie de Lyon, CNRS UMR 5276, Université Claude Bernard Lyon 1, France

²Institut Universitaire de France, France

³UMR CEA/CNRS/UVSQ 8212, LSCE, Université de Versailles – Saint-Quentin, France

⁴Laboratoire de Biométrie et Biologie Évolutive, CNRS UMR 5558, Université Claude Bernard Lyon 1, France

⁵Ecole Normale Supérieure, CERES-ERTI & LMD, France

⁶Lamont-Doherty Earth Observatory of Columbia University, Palisades, NY, USA

Corresponding author:

Christophe Lécuyer, Laboratoire de Géologie de Lyon, CNRS UMR 5276, Université Claude Bernard Lyon 1, 69622 Villeurbanne, France.
Email: clecuyer@univ-lyon1.fr

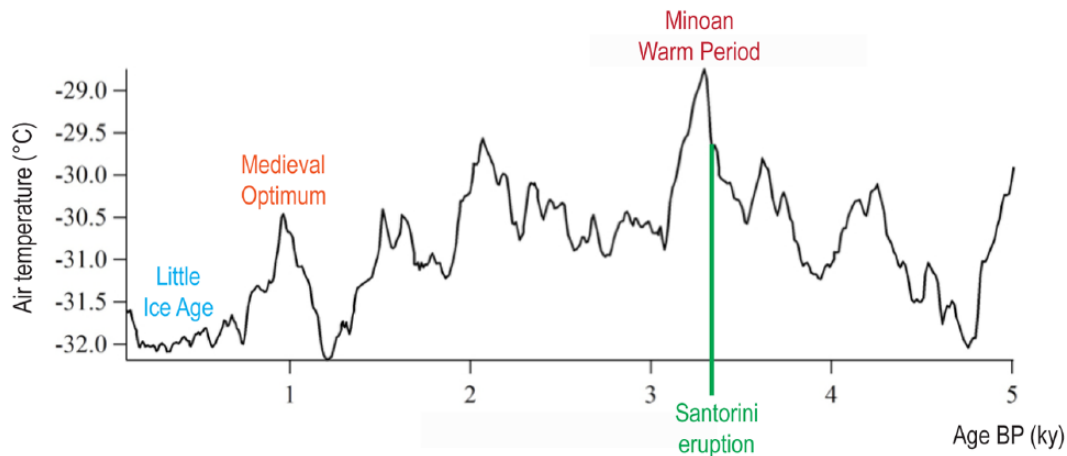


Figure 1. Variations in air temperatures over Greenland for 5000 years inferred from the stable isotope ratios (D/H; $^{18}\text{O}/^{16}\text{O}$) of ice cores (Alley, 2000). GISP2 Ice Core Temperature and Accumulation Data. IGBP PAGES/World Data Center for Paleoclimatology Data Contribution Series #2004-013. NOAA/NGDC Paleoclimatology Program, Boulder CO, USA.

Indeed, a tsunami, which means ‘harbor wave’ in Japanese, represents a series of huge shallow water waves that are able to devastate shorelines. The propagation of these waves results from the return to equilibrium subsequent to gravitational instabilities triggered by the sudden displacement of large volumes of seawater. Rapid vertical displacements of water are generally induced by submarine earthquakes resulting from the activity of reverse or thrust faults beneath subduction zones, by explosive volcanism, caldera collapse, or massive pyroclastic flows related to convergent tectonic plates.

Tsunami waves are characterized by large wavelengths from 30 to 400 km and high velocities up to 800 km h^{-1} , depending on water depth and oceanic topography (Ward, 2002). As those waves approach a coastline, they slow down and their height may increase up to about 10–15 m as their wavelength decreases to ensure the conservation of mechanical energy. Damages resulting from tsunamis are mainly caused by the high energy carried by the penetrating wave over hundreds of meters inland. Tsunami waves leave chaotic sedimentary deposits called ‘tsunamites’ of which thickness witnesses the height and the power of the tsunami wave.

This study is dedicated to the fossil faunal content of the tsunami deposit that crops out along the northeast coast of Crete (Palaikastro), Greece. Radiocarbon dating of pottery fragments and mollusc shells indicate that this tsunami was coeval with the Minoan Santorini (Thera) eruption about 3350 yr BP (Bruins et al., 2009; Manning et al., 2014) during LM1 (Bruins et al., 2008; Knappett and Cunningham, 2013). Faunal remains are abundant, taxonomically diversified, being either of marine or terrestrial origin. They include coastal marine invertebrates (bivalves, gastropods) dredged from the seabed as well as cattle skeletal remains (bones and teeth of bovinds) that accumulated during the drawback of the wave. Observations in the field, especially the measurement of the wave run-up (maximum vertical height reached inland by a tsunami above sea level), suggest that the tsunami was about 9 m high (Bruins et al., 2008) and this is comparable with the computed wave amplitude of -11.3 to 8.8 m (Novikova et al., 2011). In summary, the presence of volcanic ash, the geometry, the archeological content of the sedimentary deposits, as well as the radiocarbon dating criteria come together to indicate that the tsunami deposit was coeval with the Minoan Santorini eruption. This tsunami deposit corresponds to a climatic period globally warm during the middle Holocene, which is called ‘Minoan’ because it covers the period of rise and fall of this civilization in Crete. This period is characterized by mean temperatures warmer than those that were recorded during the 20th century (years before 1990) according to air temperatures derived

from Greenland ice core stable isotope data (Figure 1). The closest terrestrial sites to Crete, where climatic reconstructions have been made, are located in continental Greece, and they are based on pollen assemblages that reflect arid conditions (Finné et al., 2011; Kotthoff et al., 2008). Sea surface temperatures (SST) were estimated close to 25°C (against 20°C today) in the northern part of Crete about 4000 BP (Geraga et al., 2005). We performed stable oxygen isotope measurements of the faunal skeletal remains preserved in the Palaikastro tsunami deposit to reconstruct air and sea surface mean and seasonal temperatures during this so-called ‘Minoan Warm Period’.

Geological setting and sample collection

The tsunami deposit

Bruins et al. (2008) reported several lines of evidence in favor of the preservation of sedimentary, volcanic and archeological remains that are typical of tsunami deposits that can be observed at Palaikastro in north-eastern Crete, more precisely along the Chiona beach (Figure 2a and b). These sedimentary deposits are characterized by a mixture of imbricated objects of geological and archeological significance. Wall remains of Minoan buildings occur along large pebbles and stones in the lower part of the deposit, which rests unconformably on older geological strata (Figure 2c). Above the largest stony blocks, many Minoan pottery fragments occur along with volcanic ash particles, marine mollusc shells, and cattle bones.

Both ^{14}C dating and geochemical composition of the volcanic ashes revealed that they originated from the Santorini explosion 3350 ± 10 yr BP (Before Present). Santorini volcanic ashes were transported by wind from Santorini southeast to Crete just before the tsunami event. Indeed, ^{14}C dating of archeological artifacts provided similar ages of 3390 ± 60 yr BP for marine mollusc shells and 3350 ± 25 yr BP for cattle bones. During its drawback, the devastating tsunami wave has deposited a mixture of mollusc shell-bearing marine sediments and a terrestrial mud containing skeletal remains of dead animals and various artifacts belonging to the contemporaneous Minoan civilization.

Sample collection

Modern mollusc shells. A total of 50 modern molluscs were found either living or dead in less than 1 m water depth. They have been collected close to Sitia, along the Chiona beach, where crops out the tsunami deposit (Figure 2), and on the eastern coast at Kato

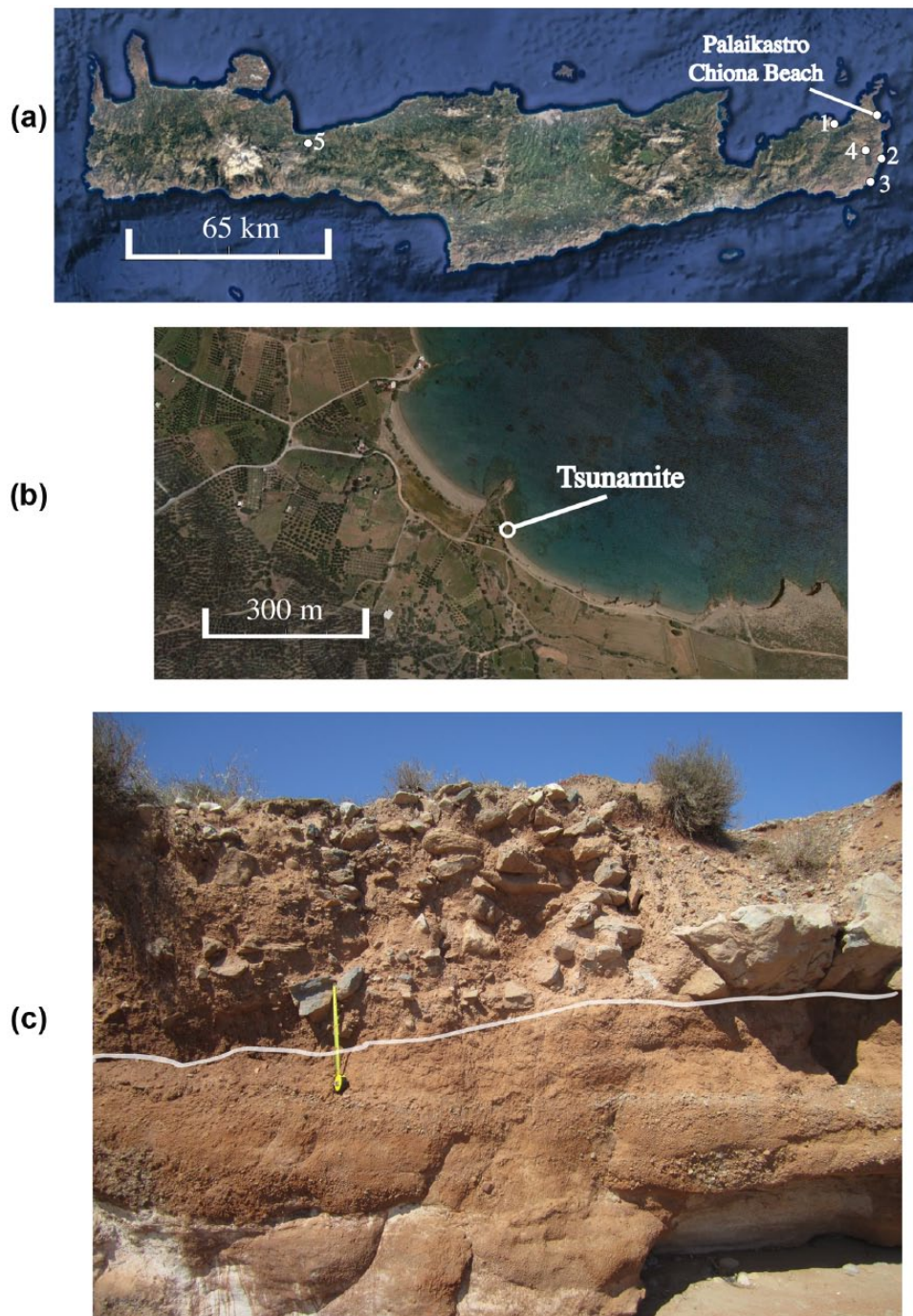


Figure 2. (a) Location of the Minoan tsunami deposit near Palaikastro, Crete, Greece, which crops out along a part of the Chiona beach. Numbers indicate the locations of water and modern mollusc sampling. (1) Sitia, (2) Kato Zakros, (3) Ambelos, (4) Zakros, and (5) Kournas Lake. (b) Chiona beach where the white dot indicates the sampling area for fossil molluscs from the tsunamite and adjacent modern molluscs and seawater. (c) The 1- to 2-m-thick upper sedimentary layer (above the white curve) was deposited by the tsunami waves generated subsequently to the explosion of the Santorini volcano about 3300 years ago. The clayey and sandy sedimentary matrix, which surround the large rocky blocks, contain numerous pottery fragments, volcanic ashes, skeletal remains from bovid, as well as well-preserved marine mollusc shells. Pictures are extracted from Google Earth®.

Zakros and Ambelos beach (Figure 2). Eroded shells were systematically discarded as they may have lived decades in the past. Collected mollusc taxa are either gastropods or bivalves. Study samples have been assigned to the following species: *Patella rustica* and *P. caerulea*, *Phocus richardi*, *Lucinoma borealis*, *Loripes lacteus*, *Fulvia fragilis*, *Arca noaea*, *Conus mediterraneus*, and *Osilinus turbinatus*.

Fossil mollusc shells and vertebrate remains. A total of 35 fossil molluscs were sampled in the tsunami deposit that crops out along Chiona beach (Figure 2b and c). Collected mollusc taxa are either gastropods or bivalves. Samples have been assigned to the

following species: *Patella caerulea*, *Conus mediterraneus*, *Osilinus turbinatus*, and *Hexaplex trunculus*. Incremental sampling of both mollusc shells and bovid tooth was performed using a diamond micro-drill (Dremel™) under a binocular.

Analytical techniques

Salinity measurements of waters

Mediterranean marine, brackish, and freshwaters of Crete were sampled during June 2012, a period of the year that matches the average annual salinity of coastal waters (Levitus et al., 1994). Conductivity of waters was measured in the field during the

collection of molluscs with a multi-parameter WTW Multi 340i™. Salinity was calculated from conductivity data according to the equation developed by Fofonoff and Millard (1983).

Hydrogen and oxygen isotope analysis of water

Aliquots of 200 mL of 14 water samples were automatically reacted at 313 K with CO₂ and H₂ in the presence of a Pt catalyst, and analyzed using a MultiPrep™ system on line with a GV IsoPrime™ dual-inlet isotope ratio mass spectrometer (IRMS). Reproducibility of δ²H and δ¹⁸O was estimated to be ±1‰ and ±0.1‰, respectively, by normalizing raw data to the isotopic ratios of VSMOW, SLAP, and GISP international standards that were measured along with the samples. When necessary, in the case of oxygen isotope ratios, a correction of −0.2‰ was applied to convert δ¹⁸O of water from the VSMOW to VPDB scales according to Bemis et al. (1998). This correction is necessary to compare measured δ¹⁸O of CO₂ produced by the reaction of the carbonate with H₃PO₄ and the CO₂ equilibrated with H₂O.

Oxygen isotope analysis of mollusc shell aragonite

Stable isotope ratios were determined by using an auto sampler MultiPrep system coupled to a dual-inlet GV IsoPrime IRMS. For bulk shells, aliquot size was about 300 µg of calcium carbonate, while they were about 10–15 µg in the case of an incremental sampling strategy. All aliquots were reacted with anhydrous over-saturated phosphoric acid at 90°C during 20 min. By default, oxygen isotope ratios of calcium carbonate are computed assuming an acid fractionation factor 1000lnα (CO₂–CaCO₃) of 8.1 between carbon dioxide and calcite (Swart et al., 1991). However, acid fractionation factors differ between aragonite and calcite as shown by Kim and O'Neil (1997) and Kim et al. (2007). At a temperature of 90°C, the mean difference in acid fractionation factors between aragonite and calcite is +0.4‰ (Kim et al., 2007). Consequently, such offset value was applied to all mollusc oxygen isotope measurements as they all made of aragonite. In addition, all sample measurements were duplicated and adjusted to the international reference NIST NBS19. External reproducibility is close to ±0.1‰ for δ¹⁸O and ±0.05 for δ¹³C (2σ) in the case of aliquots weighing ≈300 µg, while they are ±0.15 and ±0.08, respectively, in the case of small aliquots ≈10–15 µg.

Oxygen isotope analysis of apatite phosphate from vertebrate teeth and bones

Vertebrate (cattle) bone and tooth samples were treated following the chemistry procedure described by Crowson et al. (1991) and slightly modified by Lécuyer et al. (1993). This protocol isolates phosphate (PO₄^{3−}) from apatite as silver phosphate (Ag₃PO₄) crystals using acid dissolution and anion-exchange resin. After dissolution of about 10 mg of powdered apatite in 2 M HF at 25°C for 24 h, the CaF₂ precipitate was separated from the solution that included the phosphate by centrifugation. The CaF₂ precipitate was rinsed three times using DDW, then the rinse water was added to the supernate which was then neutralized with a 2 M KOH solution. Cleaned Amberjet™ resin (2 mL) was added to the neutralized solution in polypropylene tubes, which were then placed on a shaker table for 12 h to promote the ion exchange process. Excess solution was discarded and the resin was washed five times with DDW to remove the traces of ionic contaminants. To elute the phosphate ions quantitatively from the resin, 25–30 mL of 0.5 M NH₄NO₃ was added to adjust the pH of the solution to 7.5–8.5, then the tubes were gently shaken for about 4 h. Silver phosphate was precipitated from the eluted solution following the method of Firsching (1961). The solution was placed in a 250-mL Erlenmeyer flask, and about 1 mL of concentrated NH₄OH was added to raise the pH to 9–10. In total, 15 mL of ammoniacal

AgNO₃ solution was added to the flask. Upon heating this solution to 70°C in a thermostatic bath, millimeter-size yellowish crystals of Ag₃PO₄ were quantitatively precipitated. The crystals of Ag₃PO₄ were collected on a Millipore filter, washed three times with deionized distilled water (DDW), and then air dried at 50°C.

Oxygen isotope data were obtained according to a high-temperature pyrolysis continuous flow technique developed by Lécuyer et al. (2007). Aliquots of 300–500 µg of silver phosphate were mixed with 500 µg of nickelized carbon in silver foil capsules. Pyrolysis was performed at 1450°C using an Elementar VarioPYROcube™ elemental analyzer based on a 'purge and trap' technology (Fourel et al., 2011). CO is desorbed at 150°C and then transferred to a GV IsoPrime mass spectrometer in continuous flow mode with helium (He) as the carrier gas. For correction of instrumental mass fractionation during CO isotopic analysis, the δ¹⁸O of SRM 120c was fixed at 21.7‰ (VSMOW), as confirmed by published studies (e.g. Chenery et al., 2010; Halas et al., 2011; Lécuyer et al., 1993). The average standard deviation equals 0.22 ± 0.16‰. Aliquots of silver phosphate from SRM 120c were analyzed several times a day to account for possible instrument drift.

Results

Water salinity, δ¹⁸O, and δD

Coastal marine waters close to Sitia, Palaikastro, Kato Zakros, and Ambelos (Figure 2a; Table 1) have positively correlated S and δ¹⁸O ranging from 37.4‰ to 38.4‰ (g L^{−1}) and 0.90‰ to 1.18‰ (VSMOW), respectively (Table 1). Those data pairs are consistent with the absolute values and positive trend observed by Pierre (1999) for the Eastern Mediterranean Basin. Hydrogen isotope ratios of those water samples range from 7.6‰ to 11.9‰ (VSMOW) and combined to their oxygen isotope ratios they constitute a cluster defining the composition of local Mediterranean seawater being both ¹⁸O and D-enriched relative to SMOW.

Freshwaters from creeks, springs, and Kournas Lake have S and δ¹⁸O ranging from 0.19‰ to 0.62‰ and −7.72‰ to −6.76‰ (VSMOW), respectively (Table 1). δ²H–δ¹⁸O paired data (Figure 3) lie on the Mediterranean Meteoric Water Line (MMWL: δ²H = 8δ¹⁸O + 22) defined by Gat and Carmi (1970), which is distinct from the Global Meteoric Water Line (GMWL: δ²H = 8δ¹⁸O + 10) determined by Dansgaard (1964). A stagnant pond close to Zakros beach (Table 1) has the salinity of brackish waters (S = 1.96‰) with a δ¹⁸O of −6.09‰ and a δ²H of −29.7‰ (VSMOW) higher than the other sampled fresh waters (Table 1). On the basis of mass balance calculations, this brackish pond results from the mixing between 7.5 ± 0.5% of seawater and 92.5 ± 0.5% of freshwater according to the δ²H, δ¹⁸O, and S of Ambelos seawater (samples AM14 and AM15; Table 1) and Zakros freshwater (samples ZA10 and ZA11; Table 1).

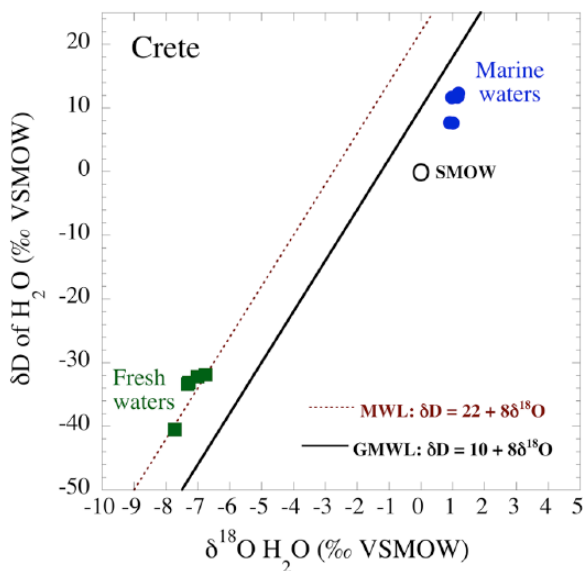
Marine mollusc shell δ¹⁸O values

Modern shells (*n* = 50) have δ¹⁸O that vary from −0.06‰ to 1.78‰ (VPDB) with a mean value of 1.13 ± 0.34‰ (Table 2), while the fossil ones (*n* = 35) sampled from the Palaikastro tsunami deposit have δ¹⁸O that lie between 0.22‰ and 1.49‰ with a mean value of 0.75 ± 0.32‰ (Table 3).

Two samples of gastropod *Osilinus turbinatus*, one modern (Table 4) and one fossil (Table 5), were incrementally sampled along their main growth axis to measure the ontogenetic evolution of their shell oxygen isotope ratios. The modern sample has oxygen isotope ratios (*n* = 30) ranging from 0.18‰ to 2.23‰ with a mean value of 1.30 ± 0.56‰, while the fossil sample has isotopic compositions (*n* = 72) in the range 0.05–2.05‰ with a mean value of 1.19 ± 0.55‰. Both samples show cyclic variations of their

Table 1. Salinity, δD , and $\delta^{18}O$ of fresh and marine waters sampled on Crete, Greece.

Sample	Location	Water origin	Geographic coordinates	S	$\delta^{18}O$	δD
				‰	‰ (VSMOW)	‰ (VSMOW)
Seawater						
CH1	Chiona beach	Open sea	N35° 11' 48.6" – E26° 16' 42.2"	37.78	1.14	11.9
CH2	Chiona beach	Open sea	N35° 11' 43.7" – E26° 16' 43.2"	38.35	1.16	11.8
CH4	Chiona beach	Open sea	N35° 11' 41.5" – E26° 16' 43.8"	38.33	1.18	12.3
CH6	Chiona beach	Open sea	N35° 11' 49.2" – E26° 16' 43.9"	38.26	1.15	11.8
SI7	Sitia	Open sea	N35° 11' 58.3" – E26° 07' 16.0"	37.96	1.14	11.8
KZ13	Kato Zakros	Open sea	N35° 06' 55.7" – E26° 13' 11.5"	37.50	0.97	11.7
AM14	Ambelos beach	Open sea	N35° 01' 41.7" – E26° 12' 31.5"	37.44	0.90	7.7
AM15	Ambelos beach	Open sea	N35° 02' 10.8" – E26° 13' 08.5"	38.10	1.00	7.6
Freshwater						
SI8	Sitia	Creek	N35° 12' 03.8" – E26° 06' 57.9"	0.36	-6.76	-31.9
SI9	Sitia	Creek	N35° 12' 11.5" – E26° 06' 40.7"	0.27	-7.01	-32.2
ZA10	Zakros	Spring	N35° 06' 55.7" – E26° 13' 11.5"	0.19	-7.28	-33.1
ZA11	Zakros	Spring	N35° 06' 53.7" – E26° 12' 41.8"	0.19	-7.32	-33.4
KZ12	Zakros	Pond	N35° 05' 44.1" – E26° 15' 44.9"	1.96	-6.09	-29.2
KO16	Kournas	Lake	N35° 06' 55.7" – E26° 13' 11.5"	0.62	-7.72	-40.5

**Figure 3.** δD – $\delta^{18}O$ space where are reported the GMWL (Dansgaard, 1964), the Mediterranean Water Line (MWL; Gat and Carmi, 1970), the SMOW reference (Craig, 1961), and the measured isotopic compositions of Crete freshwaters (green squares) and marine waters (blue circles).

oxygen isotope compositions recorded during shell growth (Tables 4 and 5).

Terrestrial vertebrate tooth and bone $\delta^{18}O$ values

Eight bone fragments of unidentified Bovidae have $\delta^{18}O$ that range from 16.3‰ to 21.3‰ (VSMOW) with a mean value of 19.1‰ (Table 6). One almost complete tooth was incrementally sampled ($n = 10$) along its growth axis; the $\delta^{18}O$ range from 18.0‰ to 22.4‰ with a mean value of 20.4‰ (Table 6).

Discussion

Preservation of the isotopic compositions

Although the studied tsunamite is very young in age at the timescale of geological processes, diagenesis of either marine molluscs shells or terrestrial vertebrate apatite may have scrambled or fully

erased the pristine oxygen isotope compositions that reflect the environmental conditions recorded during the process of skeletal mineralization. In the case of mollusc shells, x-ray diffraction analysis revealed that fossil mollusc shells have preserved their original aragonite.

Calcium phosphate has a much lower solubility than calcium carbonates. Indeed, at 25°C, solubility products (K_{sp}) equal $10^{-54.45}$ for hydroxyapatite against $10^{-8.48}$ and $10^{-6.40}$ for calcite and aragonite, respectively, according to data from JANAF thermodynamic tables. Biogenic apatite, especially tooth enamel, is generally considered as resistant to diagenetic alteration. However, the very small crystalline size of bone makes it very reactive once the collagen is gone. Under inorganic conditions and at ambient temperature, it has been shown that the oxygen isotope exchange between dissolved phosphate and water is very slow (the rate constant $k = 10^{-13}$ to 10^{-11} s $^{-1}$) and precludes any significant change in the isotopic composition of a Ca-phosphate mineral (Lécuyer et al., 1999; O'Neil et al., 2003). However, in the course of biologically mediated reactions that commonly take place during the burial of skeletal remains, the oxygen isotope compositions of apatite can be shifted by several δ units as it was observed by using modern bone and enamel powders, which were reacted at ambient temperatures with ^{13}C - and ^{18}O -labeled waters (Zazzo et al., 2004). These experiments revealed that any interpretation of apatite $\delta^{18}O$ values must remain careful. The preservation of the original isotopic signal also depends on sedimentary matrices, potential exposure of skeletal remains to post-depositional aqueous fluids, microbial activity, and the ultrastructure of the analyzed phosphatic tissues. The well-crystallized hydroxyapatite crystals, which make up tooth enamel, are large, densely packed, and constitute the most resistant phosphatic tissue to isotopic exchange with the surrounding aqueous medium. Consequently, bovid bones should be more susceptible than their teeth to diagenetic alteration because hydroxyapatite crystals of bones are smaller and less densely intergrown than those of enamel (Kolodny et al., 1996), even though several case studies have shown that the original oxygen isotope composition can be preserved in very old fossils such as Mesozoic reptile bone or dentin remains (e.g. Amiot et al., 2004; Barrick et al., 1999; Billon-Bruyat et al., 2005). On the basis of phosphate chemical yields measured during the wet chemistry procedure, clustered P_2O_5 contents from 31% to 34% indicate that the original stoichiometry of studied Minoan bovid bones was preserved and that those studied samples did not suffer significant loss (apatite dissolution) or

Table 2. Oxygen isotope compositions of modern mollusc shells from Chiona beach, Palaikastro, northeast Crete.

Sample	Location	Geographic coordinates	Taxon	$\delta^{18}\text{O}$
				‰ (VPDB)
PR-A-A-1	Ambelos beach, site 14	N35° 01' 41.7" – E26° 12' 31.5"	<i>Patella rustica</i>	1.37
PR-A-A-1	Ambelos beach, site 14	N35° 01' 41.7" – E26° 12' 31.5"	<i>Patella rustica</i>	1.58
PR-A-P-1	Chiona beach, site 1	N35° 11' 48.6" – E26° 16' 42.2"	<i>Phocus richardi</i>	1.76
PR-A-P-2	Chiona beach, site 1	N35° 11' 48.6" – E26° 16' 42.2"	<i>Phocus richardi</i>	1.00
PR-A-P-3	Chiona beach, site 1	N35° 11' 48.6" – E26° 16' 42.2"	<i>Phocus richardi</i>	1.34
Pru-A-P-1	Chiona beach, site 2	N35° 11' 43.7" – E26° 16' 43.2"	<i>Patella rustica</i>	1.31
Pru-A-P-2	Chiona beach, site 1	N35° 11' 48.6" – E26° 16' 42.2"	<i>Patella rustica</i>	1.15
Pru-A-P-3	Chiona beach, site 1	N35° 11' 48.6" – E26° 16' 42.2"	<i>Patella rustica</i>	0.59
Pru-A-P-4	Chiona beach, site 2	N35° 11' 43.7" – E26° 16' 43.2"	<i>Patella rustica</i>	1.35
Pru-A-P-5	Chiona beach, site 2	N35° 11' 43.7" – E26° 16' 43.2"	<i>Patella rustica</i>	1.27
Pru-A-P-6	Chiona beach, site 2	N35° 11' 43.7" – E26° 16' 43.2"	<i>Patella rustica</i>	0.85
PC-A-A-1	Ambelos beach, site 14	N35° 01' 41.7" – E26° 12' 31.5"	<i>Patella caerulea</i>	1.15
PC-A-A-2	Ambelos beach, site 14	N35° 01' 41.7" – E26° 12' 31.5"	<i>Patella caerulea</i>	1.06
PC-A-A-3	Ambelos beach, site 14	N35° 01' 41.7" – E26° 12' 31.5"	<i>Patella caerulea</i>	1.78
PC-A-A-4	Ambelos beach, site 14	N35° 01' 41.7" – E26° 12' 31.5"	<i>Patella caerulea</i>	1.49
PC-A-A-5	Ambelos beach, site 14	N35° 01' 41.7" – E26° 12' 31.5"	<i>Patella caerulea</i>	1.70
PC-A-A-6	Ambelos beach, site 14	N35° 01' 41.7" – E26° 12' 31.5"	<i>Patella caerulea</i>	1.42
PC-A-A-7	Ambelos beach, site 14	N35° 01' 41.7" – E26° 12' 31.5"	<i>Patella caerulea</i>	0.85
PC-A-A-8	Ambelos beach, site 14	N35° 01' 41.7" – E26° 12' 31.5"	<i>Patella caerulea</i>	-0.06
PC-A-A-9	Ambelos beach, site 14	N35° 01' 41.7" – E26° 12' 31.5"	<i>Patella caerulea</i>	0.90
LL-A-A-1	Ambelos beach, site 15	N35° 02' 10.8" – E26° 13' 08.5"	<i>Loripes lacteus</i>	1.11
LB-A-A-1	Ambelos beach, site 15	N35° 02' 10.8" – E26° 13' 08.5"	<i>Lucinoma borealis</i>	0.82
PR-A-K-1	Kato Zakros, site 13	N35° 06' 55.7" – E26° 13' 11.5"	<i>Phocus richardi</i>	1.43
PR-A-K-2	Kato Zakros, site 13	N35° 06' 55.7" – E26° 13' 11.5"	<i>Phocus richardi</i>	1.30
PR-A-K-3	Kato Zakros, site 13	N35° 06' 55.7" – E26° 13' 11.5"	<i>Phocus richardi</i>	1.17
PR-A-K-4	Kato Zakros, site 13	N35° 06' 55.7" – E26° 13' 11.5"	<i>Phocus richardi</i>	1.54
PR-A-K-5	Kato Zakros, site 13	N35° 06' 55.7" – E26° 13' 11.5"	<i>Phocus richardi</i>	1.18
PR-A-K-6	Kato Zakros, site 13	N35° 06' 55.7" – E26° 13' 11.5"	<i>Phocus richardi</i>	1.27
PR-A-K-7	Kato Zakros, site 13	N35° 06' 55.7" – E26° 13' 11.5"	<i>Phocus richardi</i>	1.36
LL-A-P-1	Chiona beach, site 1	N35° 11' 48.6" – E26° 16' 42.2"	<i>Loripes lacteus</i>	1.06
LL-A-P-2	Chiona beach, site 1	N35° 11' 48.6" – E26° 16' 42.2"	<i>Loripes lacteus</i>	0.87
LL-A-P-3	Chiona beach, site 1	N35° 11' 48.6" – E26° 16' 42.2"	<i>Loripes lacteus</i>	0.93
LL-A-P-4	Chiona beach, site 1	N35° 11' 48.6" – E26° 16' 42.2"	<i>Loripes lacteus</i>	0.70
LL-A-P-5	Chiona beach, site 1	N35° 11' 48.6" – E26° 16' 42.2"	<i>Loripes lacteus</i>	0.82
LL-A-P-6	Chiona beach, site 1	N35° 11' 48.6" – E26° 16' 42.2"	<i>Loripes lacteus</i>	1.06
FF-A-P-1	Chiona beach, site 2	N35° 11' 43.7" – E26° 16' 43.2"	<i>Fulvia fragilis</i>	0.91
FF-A-P-2	Chiona beach, site 2	N35° 11' 43.7" – E26° 16' 43.2"	<i>Fulvia fragilis</i>	0.85
FF-A-P-3	Chiona beach, site 2	N35° 11' 43.7" – E26° 16' 43.2"	<i>Fulvia fragilis</i>	0.47
FF-A-A-1	Ambelos beach, site 15	N35° 02' 10.8" – E26° 13' 08.5"	<i>Fulvia fragilis</i>	1.07
FF-A-A-2	Ambelos beach, site 15	N35° 02' 10.8" – E26° 13' 08.5"	<i>Fulvia fragilis</i>	1.47
CM-A-P-1	Chiona beach, site 1	N35° 11' 48.6" – E26° 16' 42.2"	<i>Conus mediterraneus</i>	0.61
AN-A-P-1	Chiona beach, site 2	N35° 11' 43.7" – E26° 16' 43.2"	<i>Arca noae</i>	1.53
AN-A-P-2	Chiona beach, site 2	N35° 11' 43.7" – E26° 16' 43.2"	<i>Arca noae</i>	1.26
AN-A-P-3	Chiona beach, site 1	N35° 11' 48.6" – E26° 16' 42.2"	<i>Arca noae</i>	1.12
AN-A-P-4	Chiona beach, site 1	N35° 11' 48.6" – E26° 16' 42.2"	<i>Arca noae</i>	1.17
AN-A-A-1	Ambelos beach, site 15	N35° 02' 10.8" – E26° 13' 08.5"	<i>Arca noae</i>	0.97
OT-A-A-1 ^a	Ambelos beach, site 15	N35° 02' 10.8" – E26° 13' 08.5"	<i>Osilinus turbinatus</i>	1.30
OT-A-S-1	Sitia, site 7	N35° 11' 58.3" – E26° 07' 16.0"	<i>Osilinus turbinatus</i>	1.12
OT-A-S-2	Sitia, site 7	N35° 11' 58.3" – E26° 07' 16.0"	<i>Osilinus turbinatus</i>	1.19
OT-A-S-3	Sitia, site 7	N35° 11' 58.3" – E26° 07' 16.0"	<i>Osilinus turbinatus</i>	1.26

^aIsotopic values calculated from growth isotopic profiles (see Tables 4 and 5).

addition (crystallization of secondary apatite) of exotic sources of phosphate in the tsunami deposit.

Both direction and magnitude of changes in the $\delta^{18}\text{O}$ of apatite phosphate can be estimated by using a simple mass balance calculation that takes into account a temperature-dependent oxygen isotope fractionation factor. Oxygen isotope ratios of bovid teeth result from an isotopic fractionation between the mineralized phosphate and body water at a temperature close to 37°C. Once the animal is dead, the tooth buried in the soil may react with

ambient waters through dissolution-recrystallization processes at a temperature corresponding to the local climatic conditions. In this situation, another isotopic fractionation equation must be considered and which takes into account both ambient T and $\delta^{18}\text{O}$ of water (Kolodny et al., 1996).

The variables that need to be considered are the following: (1) the water (*W*)–apatite (*A*) mass ratio (*W/A*); (2) the temperature prevailing during the isotopic exchange; (3) the oxygen isotope composition of phosphate before reaction (initial stage = $\delta(A_0)$);

Table 3. Oxygen isotope compositions of Minoan mollusc shells from Chiona beach tsunami deposit, Palaikastro, northeast Crete.

Sample	Location	Geographic coordinates	Taxon	$\delta^{18}\text{O}$
				‰ (VPDB)
OT-F-P-1	Chiona beach, site 1	N35° 11' 48.6" – E26° 16' 42.2"	<i>Osilinus turbinatus</i>	1.27
OT-F-P-2	Chiona beach, site 1	N35° 11' 48.6" – E26° 16' 42.2"	<i>Osilinus turbinatus</i>	0.87
OT-F-P-3	Chiona beach, site 1	N35° 11' 48.6" – E26° 16' 42.2"	<i>Osilinus turbinatus</i>	0.31
OT-F-P-4 ^a	Chiona beach, site 1	N35° 11' 48.6" – E26° 16' 42.2"	<i>Osilinus turbinatus</i>	1.19
PC-F-P-1	Chiona beach, site 1	N35° 11' 48.6" – E26° 16' 42.2"	<i>Patella caerulea</i>	0.95
PC-F-P-2	Chiona beach, site 1	N35° 11' 48.6" – E26° 16' 42.2"	<i>Patella caerulea</i>	1.31
PC-F-P-3	Chiona beach, site 1	N35° 11' 48.6" – E26° 16' 42.2"	<i>Patella caerulea</i>	1.49
PC-F-P-4	Chiona beach, site 1	N35° 11' 48.6" – E26° 16' 42.2"	<i>Patella caerulea</i>	1.17
PC-F-P-5	Chiona beach, site 1	N35° 11' 48.6" – E26° 16' 42.2"	<i>Patella caerulea</i>	0.88
PC-F-P-6	Chiona beach, site 1	N35° 11' 48.6" – E26° 16' 42.2"	<i>Patella caerulea</i>	0.89
MT-F-P-1	Chiona beach, site 1	N35° 11' 48.6" – E26° 16' 42.2"	<i>Murex trunculus</i>	0.98
MT-F-P-2	Chiona beach, site 1	N35° 11' 48.6" – E26° 16' 42.2"	<i>Murex trunculus</i>	0.71
MT-F-P-3	Chiona beach, site 1	N35° 11' 48.6" – E26° 16' 42.2"	<i>Murex trunculus</i>	0.68
MT-F-P-4	Chiona beach, site 1	N35° 11' 48.6" – E26° 16' 42.2"	<i>Murex trunculus</i>	0.22
MT-F-P-5	Chiona beach, site 1	N35° 11' 48.6" – E26° 16' 42.2"	<i>Murex trunculus</i>	0.59
MT-F-P-6	Chiona beach, site 1	N35° 11' 48.6" – E26° 16' 42.2"	<i>Murex trunculus</i>	1.15
MT-F-P-7	Chiona beach, site 1	N35° 11' 48.6" – E26° 16' 42.2"	<i>Murex trunculus</i>	0.43
MT-F-P-8	Chiona beach, site 1	N35° 11' 48.6" – E26° 16' 42.2"	<i>Murex trunculus</i>	0.69
MT-F-P-9	Chiona beach, site 1	N35° 11' 48.6" – E26° 16' 42.2"	<i>Murex trunculus</i>	0.86
MT-F-P-10	Chiona beach, site 1	N35° 11' 48.6" – E26° 16' 42.2"	<i>Murex trunculus</i>	0.98
MT-F-P-11	Chiona beach, site 1	N35° 11' 48.6" – E26° 16' 42.2"	<i>Murex trunculus</i>	0.47
MT-F-P-12	Chiona beach, site 1	N35° 11' 48.6" – E26° 16' 42.2"	<i>Murex trunculus</i>	0.80
MT-F-P-13	Chiona beach, site 1	N35° 11' 48.6" – E26° 16' 42.2"	<i>Murex trunculus</i>	0.27
MT-F-P-14	Chiona beach, site 1	N35° 11' 48.6" – E26° 16' 42.2"	<i>Murex trunculus</i>	0.63
MT-F-P-15	Chiona beach, site 1	N35° 11' 48.6" – E26° 16' 42.2"	<i>Murex trunculus</i>	0.55
MT-F-P-16	Chiona beach, site 2	N35° 11' 43.7" – E26° 16' 43.2"	<i>Murex trunculus</i>	0.84
MT-F-P-17	Chiona beach, site 2	N35° 11' 43.7" – E26° 16' 43.2"	<i>Murex trunculus</i>	0.62
MT-F-P-18	Chiona beach, site 2	N35° 11' 43.7" – E26° 16' 43.2"	<i>Murex trunculus</i>	0.68
MT-F-P-19	Chiona beach, site 2	N35° 11' 43.7" – E26° 16' 43.2"	<i>Murex trunculus</i>	0.74
MT-F-P-20	Chiona beach, site 2	N35° 11' 43.7" – E26° 16' 43.2"	<i>Murex trunculus</i>	0.40
MT-F-P-21	Chiona beach, site 2	N35° 11' 43.7" – E26° 16' 43.2"	<i>Murex trunculus</i>	0.34
MT-F-P-22	Chiona beach, site 2	N35° 11' 43.7" – E26° 16' 43.2"	<i>Murex trunculus</i>	0.83
MT-F-P-23	Chiona beach, site 2	N35° 11' 43.7" – E26° 16' 43.2"	<i>Murex trunculus</i>	0.45
MT-F-P-24	Chiona beach, site 2	N35° 11' 43.7" – E26° 16' 43.2"	<i>Murex trunculus</i>	0.53
CM-F-P-1	Chiona beach, site 2	N35° 11' 43.7" – E26° 16' 43.2"	<i>Conus mediterraneus</i>	0.46

^aIsotopic values calculated from ontogenetic isotopic profiles (see Tables 4 and 5).

(4) the oxygen isotope composition of phosphate after reaction (final stage = $\delta(A)$); (5) the oxygen isotope composition of water before reaction (initial stage = $\delta(\text{H}_2\text{O})_0$); (6) $[\text{O}]_W$ and $[\text{O}]_A$ are the mass fractions of oxygen in water and apatite, respectively; and (7) the oxygen isotope composition of water after reaction (final stage = $\delta(\text{H}_2\text{O})$), which can be calculated by considering $\delta(M) - \delta(\text{H}_2\text{O}) = \Delta_{A-\text{H}_2\text{O}}$; $\Delta_{A-\text{H}_2\text{O}}$ being the oxygen isotope fractionation value deduced from the isotopic fractionation equation proposed either by Kolodny et al. (1983) or by Lécuyer et al. (2013). Considering the law of mass conservation between the initial and final stages of the isotopic exchange reaction, the following relationship can be established:

$$\begin{aligned} W \times [\text{O}]_W \times \delta(\text{H}_2\text{O})_0 + A \times [\text{O}]_A \times \delta(A)_0 = \\ W \times [\text{O}]_W \times \delta(\text{H}_2\text{O}) + A \times [\text{O}]_A \times \delta(A) \end{aligned} \quad (1)$$

and re-arranged to the following expression:

$$\frac{W}{A} = \frac{[\text{O}]_A}{[\text{O}]_W} \times \left[\frac{\delta(A) - \delta(A)_0}{\delta(\text{H}_2\text{O})_0 - \delta(A) + \Delta_{A-\text{H}_2\text{O}}} \right] \quad (2)$$

Following, for example, the hypothesis of a bovid that had an initial $\delta^{18}\text{O}$ of either 18‰ or 22‰ (VSMOW), it means that it drank waters whose $\delta^{18}\text{O}$ were –2‰ (very warm and dry climate)

and –6.5‰ (present-day situation), respectively, according to the equation determined by Amiot et al. (2004). After the burial of teeth in the paleosol of Palaikastro, this hypothetical bovid tooth apatite started reacting at a temperature in the range 20–25°C with meteoric waters having negative $\delta^{18}\text{O}$ in the range –10‰ to –4‰ (VSMOW) according to both potential climate changes and the altitude at which precipitation occurs. The mass balance of Eq. (2) developed above predicts that the oxygen isotope compositions of this hypothetical bovid tooth should decrease down to 13‰ in the temperature range 20–25°C for water–apatite ratios equal or higher than 1. Such modeled $\delta^{18}\text{O}$ values are not observed among the studied fossils. Therefore they argue in favor of a rather good preservation of the pristine oxygen isotope compositions of the tooth apatite phosphate, at least sufficient to be able to relate them to their regional climatic environment. However, bone $\delta^{18}\text{O}$ are lower than those observed intra-tooth (Table 6) with a global shift of +1‰ between the tooth and the eight analyzed bone samples. We also must to take into account that bones and teeth may have been mineralized during different years prior to the tsunami event.

Estimation of marine temperatures and their seasonal variations

Method. The measurement of oxygen isotope ratios of the shell-forming aragonite from modern mollusc shells and those of their

Table 4. Oxygen isotope compositions of aragonitic external shell increments of a modern gastropod (*Osilinus turbinatus*) sampled in the coastal marine waters of northeast Crete (Palaikastro, Chiona beach).

Sample name	$\delta^{18}\text{O}$
OT-A-A-1	‰ (VPDB)
OT-A-A-1-1	0.72
OT-A-A-1-2	0.57
OT-A-A-1-4	0.18
OT-A-A-1-5	0.74
OT-A-A-1-6	1.33
OT-A-A-1-7	1.47
OT-A-A-1-8	0.88
OT-A-A-1-9	1.41
OT-A-A-1-10	1.46
OT-A-A-1-11	1.44
OT-A-A-1-12	1.33
OT-A-A-1-13	0.49
OT-A-A-1-15	0.29
OT-A-A-1-16	1.12
OT-A-A-1-17	1.88
OT-A-A-1-18	1.51
OT-A-A-1-19	1.97
OT-A-A-1-20	1.65
OT-A-A-1-21	2.07
OT-A-A-1-22	2.08
OT-A-A-1-23	2.23
OT-A-A-1-24	1.70
OT-A-A-1-25	2.18
OT-A-A-1-26	1.85
OT-A-A-1-27	0.99
OT-A-A-1-28	0.83
OT-A-A-1-29	1.08
OT-A-A-1-30	1.36
OT-A-A-1-31	1.05
OT-A-A-1-32	1.18

Table 5. Oxygen isotope compositions of aragonitic external shell increments of a Minoan gastropod (*Osilinus turbinatus*) sampled in the tsunami sedimentary deposit cropping out along the Chiona beach, Palaikastro, northeast Crete.

Sample name	$\delta^{18}\text{O}$
OT-F-P-4	‰ (VPDB)
OT-F-P-4-1	0.18
OT-F-P-4-2	0.87
OT-F-P-4-3	1.97
OT-F-P-4-4	1.62
OT-F-P-4-5	1.39
OT-F-P-4-6	1.72
OT-F-P-4-7	1.30
OT-F-P-4-8	1.84
OT-F-P-4-9	1.52
OT-F-P-4-10	1.26
OT-F-P-4-11	1.15
OT-F-P-4-12	1.79
OT-F-P-4-13	1.31
OT-F-P-4-14	1.67
OT-F-P-4-15	1.64
OT-F-P-4-16	1.46
OT-F-P-4-17	1.70
OT-F-P-4-18	1.65
OT-F-P-4-19	1.82
OT-F-P-4-20	1.73
OT-F-P-4-21	1.20

Table 5. (Continued)

Sample name	$\delta^{18}\text{O}$
OT-F-P-4-22	1.10
OT-F-P-4-23	1.59
OT-F-P-4-24	1.86
OT-F-P-4-25	1.74
OT-F-P-4-26	1.73
OT-F-P-4-27	1.61
OT-F-P-4-28	1.59
OT-F-P-4-29	1.64
OT-F-P-4-30	1.55
OT-F-P-4-31	1.46
OT-F-P-4-32	1.40
OT-F-P-4-33	1.15
OT-F-P-4-34	1.26
OT-F-P-4-35	1.15
OT-F-P-4-36	0.93
OT-F-P-4-37	0.70
OT-F-P-4-38	0.55
OT-F-P-4-39	0.37
OT-F-P-4-40	0.44
OT-F-P-4-41	0.50
OT-F-P-4-42	0.32
OT-F-P-4-43	0.30
OT-F-P-4-44	0.05
OT-F-P-4-45	0.26
OT-F-P-4-46	0.29
OT-F-P-4-47	0.69
OT-F-P-4-48	0.33
OT-F-P-4-49	0.40
OT-F-P-4-50	0.58
OT-F-P-4-51	1.05
OT-F-P-4-52	1.42
OT-F-P-4-53	1.87
OT-F-P-4-54	2.05
OT-F-P-4-56	1.72
OT-F-P-4-57	1.34
OT-F-P-4-58	0.94
OT-F-P-4-59	0.75
OT-F-P-4-60	0.29
OT-F-P-4-61	0.24
OT-F-P-4-62	0.67
OT-F-P-4-63	1.31
OT-F-P-4-64	1.77
OT-F-P-4-65	1.65
OT-F-P-4-66	1.74
OT-F-P-4-67	1.52
OT-F-P-4-68	1.52
OT-F-P-4-69	1.31
OT-F-P-4-70	1.11
OT-F-P-4-71	0.91
OT-F-P-4-72	0.61
OT-F-P-4-73	1.54

living coastal waters provided quantitative estimates of the temperature of shallow marine waters. Water temperatures were calculated by using the oxygen isotope fractionation equations that were determined between aragonite and water (Grossman and Ku, 1986; Kim et al., 2007). Those temperature estimates were also validated by comparing them with the mean annual marine temperatures that are available in the oceanographic databases (e.g. National Oceanic and Atmospheric Administration (NOAA), World Ocean Atlas).

The calculation of marine paleotemperatures using the $\delta^{18}\text{O}$ of mollusc shells requires the knowledge of the past oxygen isotope

Table 6. Oxygen isotope compositions of apatite phosphate from eight bone fragments of Minoan bovids and 10 increments of enamel sampled along the growth axis of one Minoan bovid tooth (Figure 11).

Sample reference	$\delta^{18}\text{O}_p$ ‰ (VSMOW)
Bone fragments	
OS_FP_1	16.93
OS_FP_2	16.25
OS_FP_3	18.04
OS_FP_4	19.43
OS_FP_5	20.88
OS_FP_6	20.67
OS_FP_7	21.27
OS_FP_8	18.94
Tooth enamel	
DEF-P1	21.63
DEF-P2	17.99
DEF-P3	18.90
DEF-P4	20.59
DEF-P5	18.83
DEF-P6	21.93
DEF-P7	20.91
DEF-P8	21.14
DEF-P9	22.38
DEF-P10	19.88

composition of seawater. Assuming that the oxygen isotope composition of Mediterranean seawater 3350 years ago was similar to today is a robust hypothesis. Indeed, the $\delta^{18}\text{O}$ of a water mass reflects its hydrological budget and that of Mediterranean Sea has been considered at steady state for at least 6000 years (Emeis et al., 2003). Therefore, the $\delta^{18}\text{O}$ measured for the coastal seawater of Crete are used to calculate the paleotemperatures inferred from the oxygen isotope compositions of the unearthed mollusc shells.

Besides these calculated mean seawater temperature data, the incremental oxygen isotope analysis performed along the main growth axis of gastropod shells (Trochidae, Patellidae, Muricidae) allowed seasonal temperature variations to be reconstructed. These high-temporal resolution data are critical to determine the regional climatic mode as they indeed reflect seasonal changes in solar radiation and prevailing winds. Temperature seasonality also partly controls the marine biodiversity.

The exoskeleton growth of most mollusc species is logarithmic instead of linear (e.g. Cornu et al., 1993; Hernandez-Llamas and Ratkowsky, 2004; Román-Román et al., 2010; Von Bertalanffy, 1938). The input signal describing the seasonal temperature variations, which is sinusoidal, is thus distorted. The record of time thus appears stretched during the juvenile stage of the mollusc, which is characterized by rapid growth, and contracted when approaching the mature stage. Some mollusc species are characterized by a growth rate depending on the surrounding water temperature, which may become very low even null below or above some threshold values. The input signal, that is, the oscillating water temperature, may thus also be distorted with the maxima and minima of the sinusoidal variations being truncated as the result of an absence of mineralization, which means no record during those periods of the year.

Interpretation. Regional (northeast Crete) SST were calculated by using two oxygen isotope fractionation equations for the aragonite–water system (Figure 4). The first one (Figure 4a) was determined by analyzing modern molluscs and ambient water in

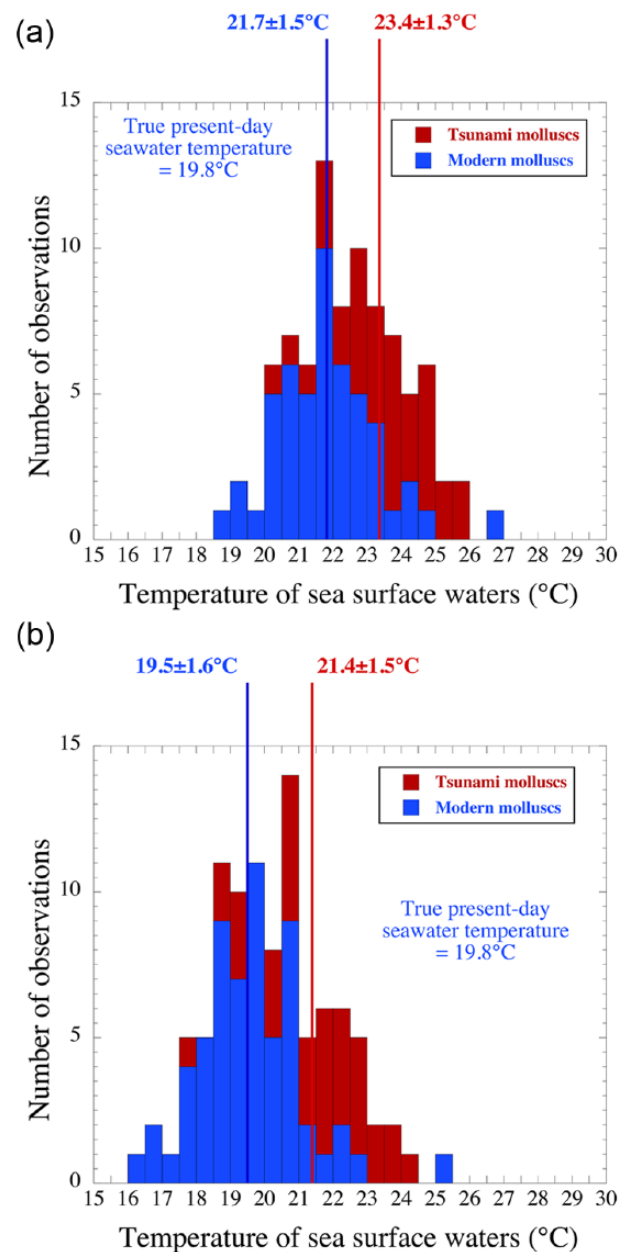


Figure 4. Modern (blue) and Minoan (red) temperatures of sea surface waters calculated by using the $\delta^{18}\text{O}$ of mollusc shells and coastal marine waters from northeast Crete (Palaikastro, Chiona beach) according to the aragonite–water oxygen isotope fractionation equations determined by (a) Grossman and Ku (1986) and (b) Kim et al. (2007).

the temperature range $\approx 3\text{--}15^\circ\text{C}$ (Grossman and Ku, 1986), while the second one (Figure 4b) was obtained from laboratory experiments (Kim et al., 2007). The best match between true SST and calculated ones was obtained by applying Kim et al. (2007) equation to our set of data (Figure 4b). Indeed, the calculated mean SST of $19.5 \pm 1.6^\circ\text{C}$ is close to the mean sea surface isotherm (20.2°C) that reaches the eastern coast of Crete (Figure 5a) as well as the mean SST of 19.8°C close to Heraklion (Figure 5b). It is worthy to note that the use of (Grossman and Ku, 1986) equation allows the mean SST to be overestimated by about 2°C . Therefore, we used Kim et al. (2007) equation to infer the SST that prevailed ≈ 3350 yr BP. Calculated temperatures were about 2°C higher than during the end of the 20th century and characterized by a similar standard deviation of $\pm 1.5^\circ\text{C}$ (2σ). A Welch two sample *t*-test rejects the null hypothesis (means are not significantly different) with a probability of 8.5×10^{-7} . Similar standard

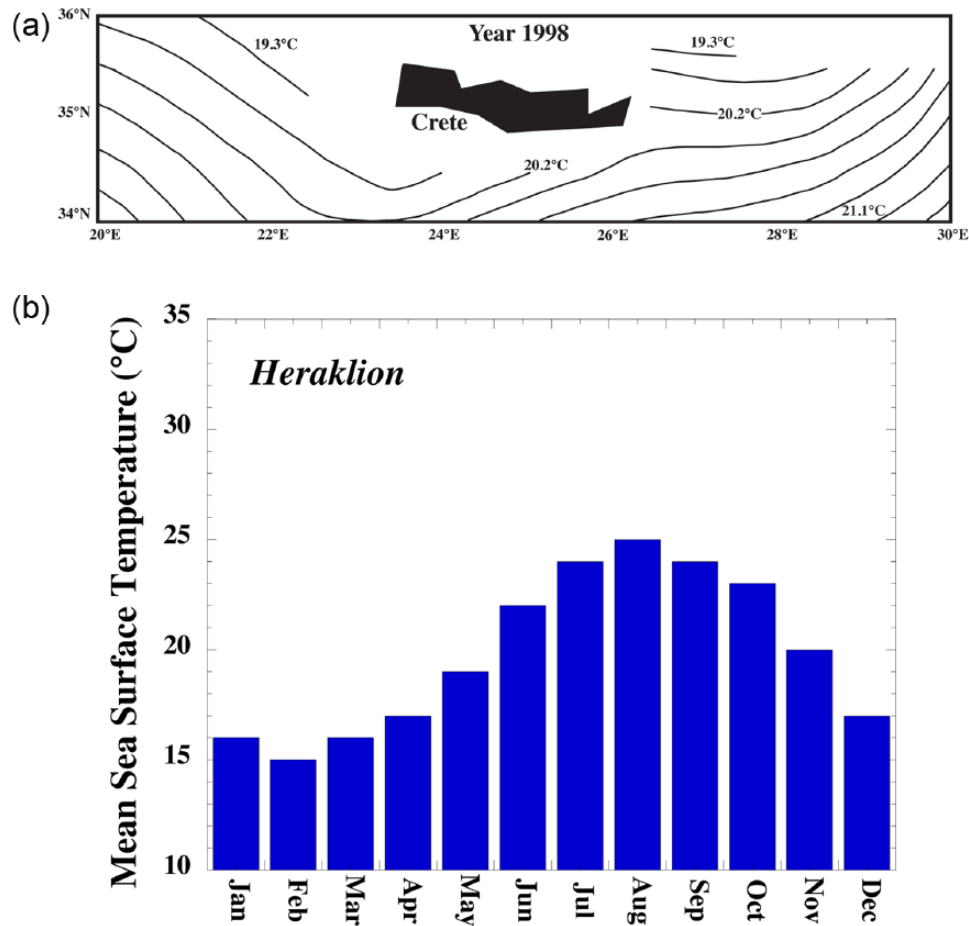


Figure 5. (a) Sea surface isotherms around the island of Crete for the year 1998 and (b) seasonal variations in mean SST for the last 20 years at Heraklion, Crete. The coldest month is February, while the warmest one is August. Data come from NOAA/WMO.

deviations most likely reflect that collected molluscs, in both cases, integrated inter-annual SST variations, perhaps over several decades, as they most likely did not die at the same time. Consequently, on the basis of these data, we propose that Crete SST during the ‘Warm Minoan Period’ were higher by about 2°C than during the second half of the last century.

Ontogenetic profiles of the modern and fossil *Osilinus turbinatus* (Figure 6a and b) show strong isotopic variations that could be related to seasonal (sinusoidal-like) fluctuations of the SST when taking into account the non-linear skeletal growth of mollusc shells. Such distortion of the input signal during the shell growth is especially obvious for sample OT-F-P-4 (Figure 6b) that is more pronounced than for the modern *O. turbinatus* and that allowed more time to be recorded (Figure 6a). Indeed, as predicted by the theory, the isotopic record appears stretched during the juvenile stage (fast growth) of the mollusc, whereas it appears contracted when approaching the mature stage (slow growth). The isotopic curves do not show any evidence of truncated records that could lead to underestimation of the seasonal amplitude especially during the cold season when the mollusc metabolism is lowered. On the basis of those modern and fossil samples, no significant differences can be observed either in terms of mean SST between the modern ($T = 19.2^{\circ}\text{C}$ and 19.7°C , respectively) or seasonal amplitude A ($A = 9.8^{\circ}\text{C}$ and 9.6°C , respectively). These values compare well with the present-day true mean temperature and seasonal amplitude at Heraklion, which are $\approx 19.8^{\circ}\text{C}$ and 10°C , respectively (Figure 5b). These temperature estimates obtained from single specimens could be considered at variance with those inferred from the 35 bulk shell $\delta^{18}\text{O}$. However, those bulk values are most likely more robust proxies of mean SST as they smooth potential inter-annual temperature variations and

intra-population variability because of differences in the individual environments and maybe to individual metabolic differences.

Estimation of terrestrial temperatures and their seasonal variations

Method. The D/H and $^{18}\text{O}/^{16}\text{O}$ ratios of precipitation are potentially good climatic indicators at this latitude. Above all, if they reflect the sources and trajectories of humid air masses, they also allow air temperatures to be estimated at the seasonal or multi-annual scale in a given area, taken into account the possible altitude effects. In Crete, the mean annual air temperature is close to 19°C at sea level (Figure 7), the precipitations mainly occurring at high elevation during the autumn and winter, more precisely from October to March with a mean monthly precipitation of 70 mm (Figure 8). Their oxygen isotope ratios are strongly influenced by the mountains that play an important role in the condensation of humid air masses (Vrochidou and Tsanis, 2012). On this island, at sea level, the mean $\delta^{18}\text{O}$ of meteoric waters is close to -5.5% (SMOW), while at 800 m altitude, it is close to -7.5% (Dotsika et al., 2010). Spring waters represent an important source of drinking water for human beings and cattle, those documented in the framework of this study have $\delta^{18}\text{O}$ close to -7% (-7.3% to -6.8% ; Table 1), thus suggesting that the spring waters we analyzed were formed at altitudes close to 500–700 m in the north-east of Crete (Figure 9), and at air temperatures lower by about 4°C in average than those prevailing near sea level (Matzarakis and Nastos, 2011).

A relationship between the $\delta^{18}\text{O}$ of meteoric waters and mean air temperature (MAT), which is the so-called ‘Global Meteoric Water Line’ was determined by Dansgaard (1964):

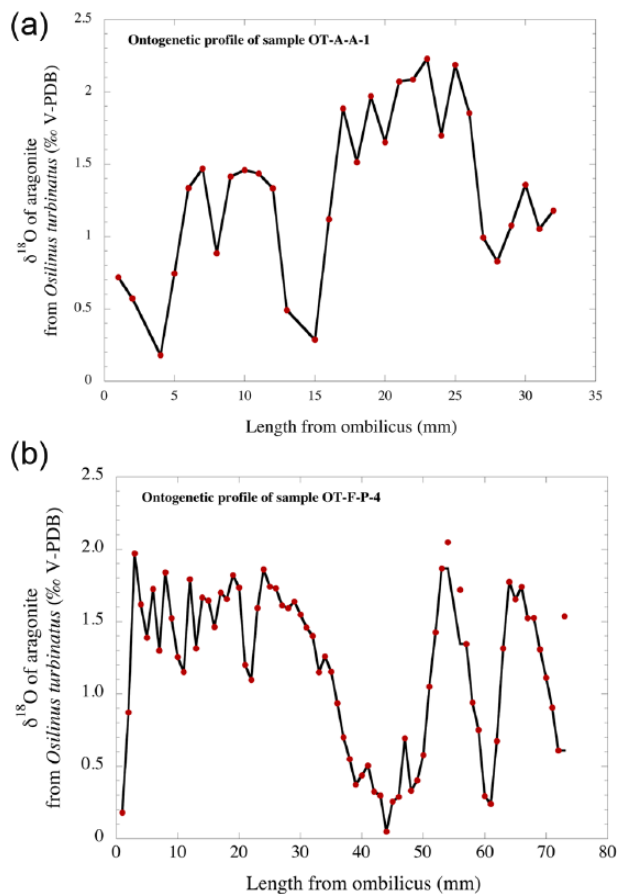


Figure 6. Oxygen isotope records of growth of aragonitic shells from (a) modern (sample OT-A-A-1) and (b) Minoan (sample OT-F-P-4) *Ostilinus turbinatus*, Palaikastro, northeast Crete.

$$\delta^{18}\text{O} = 8.1 \times \delta^2\text{H} + 11 \quad (3)$$

However, the slope and intercept of such a linear relationship may vary at the regional scale depending on the topography, the vicinity of oceans, and the climate mode. Thus, the Mediterranean Basin is characterized by a linear equation distinct from GMWL (Gat and Carmi, 1970):

$$\delta^{18}\text{O} = 8 \times \delta^2\text{H} + 22 \quad (4)$$

Consequently, a distinct relationship (5) between the MAT (°C) and the oxygen isotope composition of meteoric waters ($\delta^{18}\text{O}_{\text{mw}}$) is determined for the Mediterranean Basin (Figure 10a) and compared with Eq. (6) established by Lécuyer (2014) for the European areas spared by the influence of the Mediterranean climate mode:

$$\text{MAT}(\text{°C}) = 1.72(\pm 0.22) \times \delta^{18}\text{O}_{\text{mw}} + 25.87(\pm 1.13) \quad (5)$$

$$\text{MAT}(\text{°C}) = 1.41(\pm 0.09) \times \delta^{18}\text{O}_{\text{mw}} + 22.02(\pm 0.83) \quad (6)$$

For example, considering a similar value for the mean $\delta^{18}\text{O}$ of meteoric waters, the use of Eq. (6) leads to an underestimation by about 2°C of the MAT in the Mediterranean Basin. Consequently, Eq. (5) was preferred to estimate the MATs from the oxygen isotope compositions of meteoric waters. In addition, a second equation (7) can be established by using the data (IAEA, WMO database) collected between 1960 and 1981 at Heraklion:

$$\text{MAT}(\text{°C}) = 2.34(\pm 0.62) \times \delta^{18}\text{O}_{\text{mw}} + 28.93(\pm 3.58) \quad (7)$$

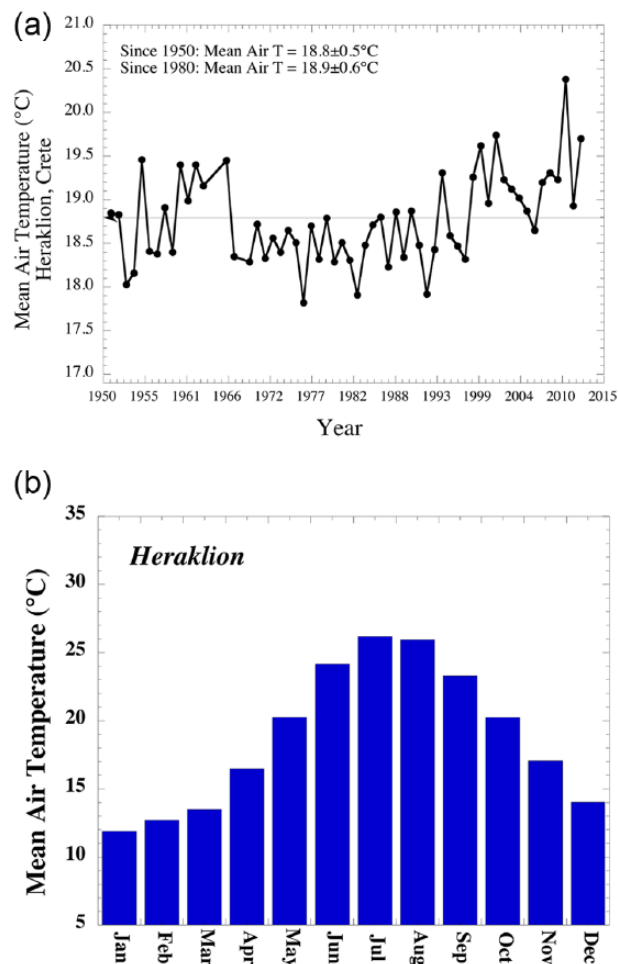


Figure 7. (a) Evolution of mean annual air temperatures (MAAT) at Heraklion, Crete, from years 1950 to 2012. (b) Seasonal variations in mean air temperatures at Heraklion, Crete. The coldest month is January, while the warmest one is July. Data come from NOAA/WMO.

Those compositions of meteoric waters constitute the main source of drinking water for vertebrates that record their oxygen isotope ratios in their mineralized tissues (bones and teeth). Thus, a general equation (8) was established between the oxygen isotope composition of meteoric waters ($\delta^{18}\text{O}_{\text{m}}$) and the $\delta^{18}\text{O}_{\text{p}}$ of phosphate ions (PO_4^{3-}) from the dahlite (also called carbonateapatite) mineral of chemical formula $\text{Ca}_{10}(\text{PO}_4, \text{CO}_3)_6(\text{OH}, \text{CO}_3)_2$ that constitutes the inorganic fraction of teeth and bones of herbivorous mammals (Amiot et al., 2004):

$$\delta^{18}\text{O}_{\text{mw}} = 1.11(\pm 0.03) \times \delta^{18}\text{O}_{\text{p}} - 26.44(\pm 0.05) \quad (8)$$

Combining Eq. (5) or (7) with Eq. (8) allowed MATs to be estimated from the oxygen isotope compositions of bovid tooth enamel and bones.

Interpretation. As bones are continuously remodeled during the animal life, they record weighted average $\delta^{18}\text{O}$ of meteoric waters. However, the lowest temperatures calculated from bone $\delta^{18}\text{O}$ using Eq. (5) (11.5–20°C) or Eq. (7) (9–22°C) cannot correspond to mean annual temperatures for an island located in the eastern Mediterranean Basin. Therefore, we interpret the $\delta^{18}\text{O}$ of vertebrate bones as the result of a diagenetic alteration that took place during burial.

The bovid tooth has a mean $\delta^{18}\text{O}$ of 20.4‰ that corresponds to a mean $\delta^{18}\text{O}_{\text{mw}}$ for meteoric waters of -3.8‰, which is greater

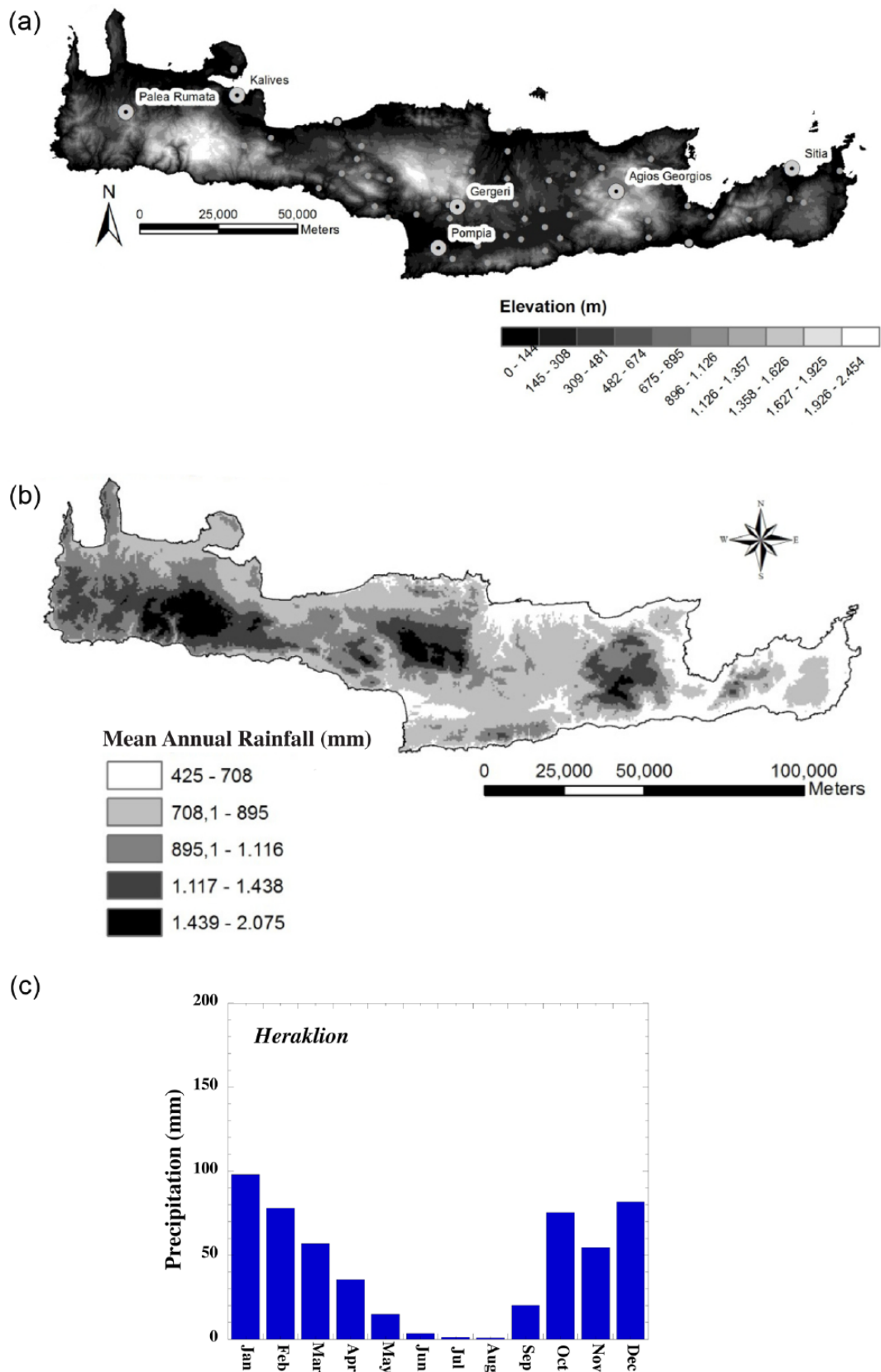


Figure 8. (a) Orographic and (b) precipitation map of Crete showing that mean annual rainfall strongly increases with elevation. Maps are derived from Vrochidou and Tsanis (2012). (c) Seasonal variations in mean monthly precipitation at Heraklion, Crete. The wettest month is January, while the driest one is August. Data come from NOAA/WMO.

than the weighted rainfall $\delta^{18}\text{O}$ of -5.7‰ recorded at Heraklion between 1960 and 1981 according to the IAEA/WMO database. MATs of 19.4°C and 20.1°C were calculated using $\delta^{18}\text{O}_{\text{mw}}$ -MAT relationships determined by compiling IAEA/WMO data from stations located around the Mediterranean Basin (Eq. (5); Figure

10a) and data restricted to Heraklion (Eq. (7); Figure 10b). Assuming that Eqs (5) and (7) may be transposed to the 'Minoan Period', both temperature estimates for the 'Minoan Period' are slightly higher than the recorded MAT at Heraklion since 1950 ($T = 18.8 \pm 0.5^{\circ}\text{C}$) or even since 1980 ($T = 18.9 \pm 0.6^{\circ}\text{C}$; Figure 7a).

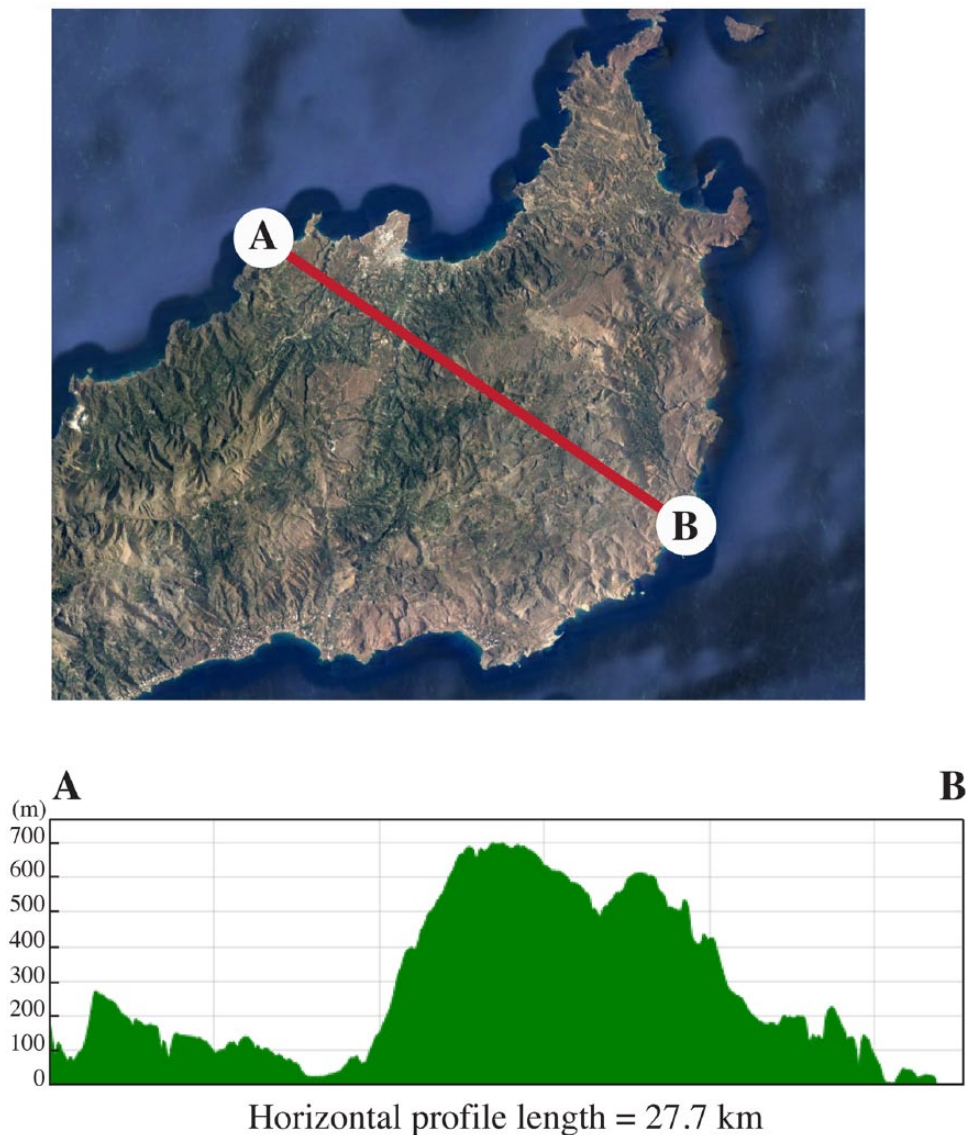


Figure 9. Topographic profile A–B across northeast Crete. Map was extracted from Google Earth®, while the topographic profile was computed using the web application ‘Geocontext-Profiler’ located at: <http://www.geocontext.org/publ/2010/04/profiler/en/>. Precipitations with $\delta^{18}\text{O}$ close to -7‰ mostly form between 500 and 700 m where mean air temperatures are in average 4°C lower than those close to sea level (Matzarakis and Nastos, 2011).

Intra-tooth variations in the oxygen isotope ratios could be assigned to the record of seasonal variations in $\delta^{18}\text{O}$ values during tooth enamel growth as already evidenced for many examples of mammals such as sheep, elk, deer, bovid, bison, or horse (e.g. Bernard et al., 2009; Fabre et al., 2011; Fricke et al., 1998; Gadbury et al., 2000; Zazzo et al., 2002). The suggested temperature seasonal range inferred from the fossil bovid tooth is either $15\text{--}23^\circ\text{C}$ using Eq. (5) (Figure 11) or $14\text{--}25^\circ\text{C}$ using Eq. (7), both ranges being more restricted than that recorded between 1961 and 1980 ($T_{\min} = 12^\circ\text{C}$ in January and $T_{\max} = 26^\circ\text{C}$ in July; Figure 7b). According to our data, winters could have been milder than nowadays but it is quite surprising to obtain cooler summers. Such odd results could be at least partly explained by a bias related to the method used in the framework of this study. Indeed, air temperatures are inferred from $\delta^{18}\text{O}$ of meteoric waters, meaning there is a relation between those values and the seasonal and geographic distributions of precipitation. Meteorological data highlight the fact that rainfalls are negligible during summer, consequently the warmest season is not recorded during tooth growth. Moreover, rainfall, mainly occurring during both winter and autumn, are strongly correlated with the orography; the higher the elevation, the higher the amount of rainfall. This observation suggests that

most of the water drunk by terrestrial vertebrates in northeast Crete comes from springs fed by rainfall formed between 500 and 700 m (Figures 8a and 9) where the temperatures are in average 4°C lower than those recorded close to the sea level (Matzarakis and Nastos, 2011). Consequently, the $\delta^{18}\text{O}$ values of meteoric waters inferred from those of mammal apatite reflect altitude temperatures and not those close to sea level.

The ‘Minoan Warm Period’ and the climate in Crete

Greenland ice cores have revealed the existence of a warm period extending from 3400 to 3250 BP, called the ‘Minoan Warm Period’, and that brackets the date of the Palaikastro tsunami deposit resulting from the eruption and collapse of the Santorini volcano about 3350 BP. Coastal surface seawater temperatures and MATs were most likely about 2°C and 4°C higher, respectively, than during the second half of the 20th century. The climatic conditions prevailing at the end of the Minoan civilization were not only significantly warmer than today but also most likely drier as suggested by the especially high $\delta^{13}\text{C}$ values analyzed in the contemporaneous sections of stalagmites from caves located in the Peloponnese Peninsula (Finné, 2014).

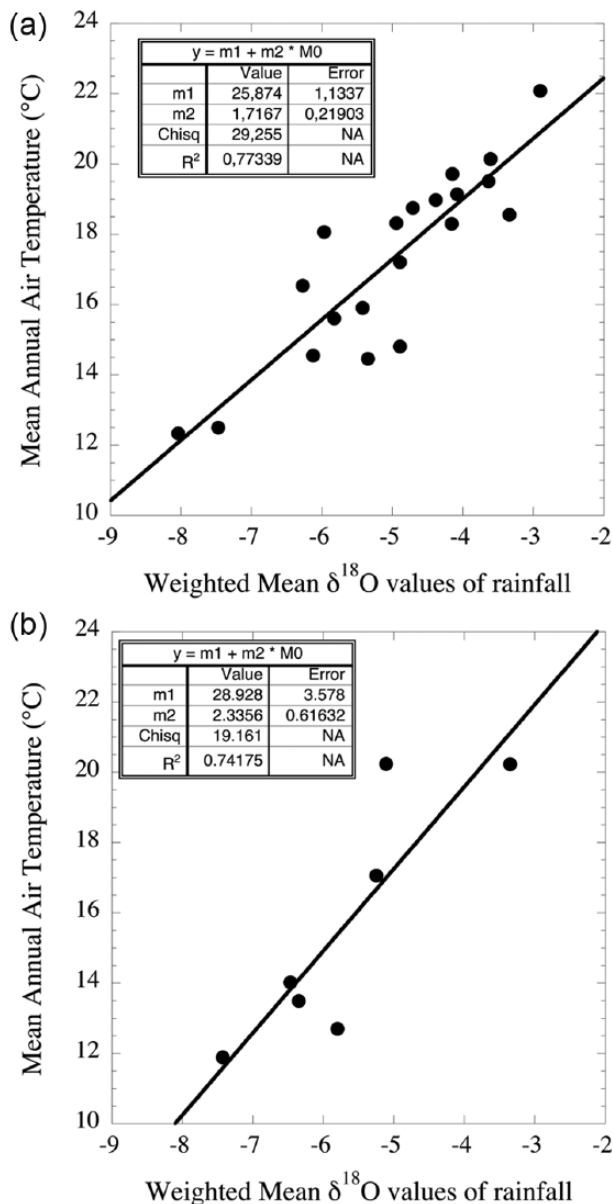


Figure 10. (a) Linear correlation equation (5) between the mean annual air temperature and the $\delta^{18}\text{O}$ of meteoric waters for the Mediterranean Basin. IAEA stations are located along the coasts of the following countries: Spain (Barcelona, Madrid), Italy (Basovizza, Feletto, Genoa, Pisa), Greece (Athens, Rhodes), Turkey (Antalya, Adana), Israel (Bet Dagan, Har Kna'An), Jordania (Amman-Waj), Egypt (Alexandria, Cairo, Sidi Barrani), Tunisia (Sfax, Tunis), Gibraltar and Morocco (Fes Sais). (b) Linear correlation equation (7) between the mean annual air temperature and the $\delta^{18}\text{O}$ of meteoric waters for Heraklion, Crete, Greece. Data come from NOAA/WMO.

Conclusion

The tsunamite that crops out along the Chiona beach near the city of Palaikastro in Crete, Greece, contains numerous mollusc shells, which were dredged from the seabed, as well as cattle skeletal remains and various artifacts belonging to the contemporaneous Minoan civilization, more precisely during MM3 and LM1 periods according to radiocarbon dating of mollusc shells and pottery fragments. Stable isotope compositions of both marine mollusc shells and terrestrial vertebrate remains allowed some climatic parameters of the 'Warm Minoan Period' to be quantified:

- Incremental sampling performed along the growth axis of a bovid tooth revealed that air temperatures were about

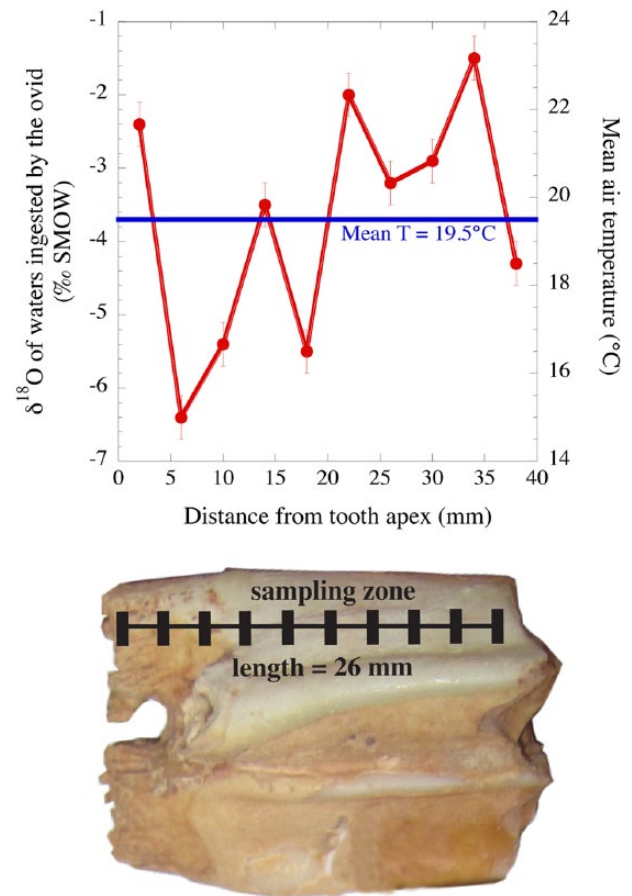


Figure 11. Oxygen isotope records of growth of tooth enamel phosphate from a Minoan bovid (sample DEF-P; Table 6). Oxygen isotope compositions of meteoric waters and air temperatures were calculated using Eqs (5) and (8).

4°C higher than during the second half of the 20th century. However, it is worthy to note that the oxygen isotope compositions of terrestrial vertebrate bone remains most likely resulted from diagenetic alteration.

- Oxygen isotope measurements of marine mollusc shells revealed that sea surface temperatures were higher by about 2°C during the same period. Incremental sampling of a marine gastropod suggests that the seasonal amplitude was similar to present-days.

While the 'Warm Minoan Period' has been recorded in both δD and $\delta^{18}\text{O}$ values of Greenland ice cores with a 2.5°C temperature difference, our study revealed that the Mediterranean Basin, at least in the Crete area, also suffered a significant warming. Drier climatic conditions were also inferred from the high $\delta^{13}\text{C}$ values of contemporaneous stalagmites from caves located in the Peloponnese Peninsula. A climatic deterioration with increasing warming and drying most likely had a drastic and lasting impact on the quality and quantity of food resources on the island. These results should be taken into account to analyze the social and political changes that took place during this period of the Minoan civilization.


Acknowledgements


The authors thank Martine Lécuyer for her help in collecting samples on the field.

Funding

The author(s) received no financial support for the research, authorship, and/or publication of this article.

ORCID iDs

Romain Amiot  <https://orcid.org/0000-0003-2779-9652>

Kevin Rey  <https://orcid.org/0000-0002-6788-2453>

References

- Alley RB (2000) The younger Dryas cold interval as viewed from central Greenland. *Quaternary Science Reviews* 19(1–5): 213–226.
- Amiot R, Lécuyer C, Buffet E et al. (2004) Latitudinal temperature gradient during the Cretaceous Upper Campanian – Middle Maastrichtian: $\delta^{18}\text{O}$ record of continental vertebrates. *Earth and Planetary Science Letters* 226: 255–272.
- Barrick RE, Fischer AG and Showers WJ (1999) Oxygen isotopes from turtle bone: Application for terrestrial paleoclimates? *PALAIOS* 14: 186–191.
- Bemis BE, Spero HJ, Bijma J et al. (1998) Reevaluation of the oxygen isotopic composition of planktonic foraminifera: Experimental results and revised paleotemperature equations. *Paleoceanography* 13(2): 150–160.
- Bernard A, Daux V, Lécuyer C et al. (2009) Pleistocene seasonal temperature variations recorded in the $\delta^{18}\text{O}$ of *Bison priscus* teeth. *Earth and Planetary Science Letters* 283: 133–143.
- Billon-Bruyat JP, Lécuyer C, Martineau F et al. (2005) Oxygen isotope compositions of Late Jurassic vertebrate remains from lithographic limestones of western Europe: Implications for the ecology of fish, turtles and crocodilians. *Palaeogeography, Palaeoclimatology, Palaeoecology* 216: 359–375.
- Bruins HJ, Van der Plicht J and MacGillivray JA (2009) The Minoan Santorini eruption and tsunami deposits in Palaikastro (Crete): Dating by geology, archeology, ^{14}C , and Egyptian chronology. *Radiocarbon* 51(2): 397–411.
- Bruins HJ, MacGillivray JA, Synolakis CE et al. (2008) Geoaerchaeological tsunami deposits at Palaikastro (Crete) and the Minoan IA eruption of Santorini. *Journal of Archaeological Science* 35: 191–212.
- Chenery C, Müldner G, Evans J et al. (2010) Strontium and stable isotope evidence for diet and mobility in Roman Gloucester, UK. *Journal of Archaeological Science* 37: 150–163.
- Cornu S, Pätzold J, Bard E et al. (1993) Paleotemperature of the last interglacial period based on $\delta^{18}\text{O}$ of *Strombus bubonius* from the western Mediterranean Sea. *Palaeogeography, Palaeoclimatology, Palaeoecology* 103: 1–20.
- Craig H (1961) Standard for reporting concentration of deuterium and oxygen-18 in natural waters. *Science* 133: 1833–1834.
- Crowson RA, Showers WJ, Wright EK et al. (1991) A method for preparation of phosphate samples for oxygen isotope analysis. *Analytical Chemistry* 63: 2397–2400.
- Dansgaard W (1964) Stable isotopes in precipitation. *Tellus* 16: 436–468.
- Dotsika E, Lykoudis S and Poutoukis D (2010) Spatial distribution of the isotopic composition of precipitation and spring water in Greece. *Global and Planetary Change* 71: 141–149.
- Emeis KC, Schulz H, Struck U et al. (2003) Eastern Mediterranean surface water temperatures and $\delta^{18}\text{O}$ composition during deposition of sapropels in the late Quaternary. *Paleoceanography* 18(1): 1005.
- Esper J, Krusic PJ, Ljungqvist FC et al. (2016) Ranking of tree-ring based temperature reconstructions of the past millennium. *Quaternary Science Reviews* 145: 134–151.
- Fabre M, Lécuyer C, Brugal JP et al. (2011) Late Pleistocene climatic change in the French Jura (Gigny) recorded in the $\delta^{18}\text{O}$ of phosphate from ungulate tooth enamel. *Quaternary Research* 75: 605–613.
- Finné M (2014) *Climate in the Eastern Mediterranean during the Holocene and beyond – A Peloponnesian perspective*. PhD Thesis, Stockholm University, 52 pp.
- Finné M, Holmgren K, Sundqvist HS et al. (2011) Climate in the eastern Mediterranean, and adjacent regions, during the past 6000 years – A review. *Journal of Archaeological Science* 39: 3153–3173.
- Firsching FH (1961) Precipitation of silver phosphate from homogeneous solution. *Analytical Chemistry* 33(7): 87–874.
- Fofonoff NP and Millard RC (1983) Algorithms for computation of fundamental properties of seawater. *UNESCO Technical Papers in Marine Science* 44: 1–53.
- Fouré F, Martineau F, Lécuyer C et al. (2011) $^{18}\text{O}/^{16}\text{O}$ ratio measurements of inorganic and organic materials by elemental analysis–pyrolysis–isotope ratio mass spectrometry continuous-flow techniques. *Rapid Communications in Mass Spectrometry* 25(19): 2691–2696.
- Fricke HC, Clyde WC and O’Neil JR (1998) Intra-tooth variations in $\delta^{18}\text{O}(\text{PO}_4)$ of mammalian tooth enamel as a record of seasonal variations in continental climate variables. *Geochimica et Cosmochimica Acta* 62(11): 1839–1850.
- Gadbury C, Todd L, Jahren AH et al. (2000) Spatial and temporal variations in the isotopic composition of bison tooth enamel from the Early Holocene Hudson-Meng Bone Bed, Nebraska. *Palaeogeography, Palaeoclimatology, Palaeoecology* 157: 79–93.
- Gat JR and Carmi I (1970) Evolution of the isotopic composition of the atmospheric water in the Mediterranean Sea area. *Journal of Geophysical Research* 75: 3039–3048.
- Geraga M, Tsaila-Monopolis S, Ioakim C et al. (2005) Short-term climate changes in the southern Aegean Sea over the last 48,000 years. *Palaeogeography, Palaeoclimatology, Palaeoecology* 220: 311–332.
- Goring S, Pellatt MG, Lacourse T et al. (2009) A new methodology for reconstructing climate and vegetation from modern pollen assemblages: An example from British Columbia. *Journal of Biogeography* 36(4): 626–638.
- Grossman EL and Ku TL (1986) Oxygen and carbon isotope fractionation in biogenic aragonite: Temperature effects. *Chemical Geology: Isotope Geoscience Section* 59: 59–74.
- Halas S, Skrzypek G, Meier-Augenstein W et al. (2011) Interlaboratory calibration of new silver orthophosphate comparison materials for the stable oxygen isotope analysis of phosphates. *Rapid Communications in Mass Spectrometry* 25(5): 579–584.
- Hernandez-Llamas A and Ratkowsky DA (2004) Growth of fishes, crustaceans, and molluscs: Estimation of the von Bertalanffy, Logistic, Gompertz and Richards curves and a new growth model. *Marine Ecology Progress Series* 282: 237–244.
- Kim ST and O’Neil JR (1997) Equilibrium and nonequilibrium oxygen isotope effects in synthetic carbonates. *Geochimica et Cosmochimica Acta* 61(16): 3461–3475.
- Kim ST, O’Neil JR, Hillaire-Marcel C et al. (2007) Oxygen isotope fractionation between synthetic aragonite and water: Influence of temperature and Mg^{2+} concentration. *Geochimica et Cosmochimica Acta* 71(19): 4704–4715.
- Knappett C and Cunningham T (2013) Defining middle Minoan IIIA and IIIB at Palaikastro. In: Knappett C and Macdonald CF (eds) *Intermezzo: Intermediacy and Regeneration in Middle Minoan III Palatial Crete* (British School at Athens Studies, vol. 21). Athens: British School at Athens, pp. 183–195.
- Kolodny Y, Luz B and Navon O (1983) Oxygen isotope variations in phosphate of biogenic apatites, I. Fish bone apatite – Rechecking the rules of the game. *Earth and Planetary Science Letters* 64: 398–404.
- Kolodny Y, Luz B, Sander M et al. (1996) Dinosaur bones: Fossils or pseudomorphs? The pitfalls of physiology reconstruction from apatitic fossils. *Palaeogeography, Palaeoclimatology, Palaeoecology* 126: 161–171.
- Kotthoff U, Müller UC, Pross J et al. (2008) Lateglacial and Holocene vegetation dynamics in the Aegean region: An integrated

- view based on pollen data from marine and terrestrial archives. *The Holocene* 18(7): 1019–1032.
- Lécuyer C (2014) *Water on Earth*. London: ISTE Ltd; New York: John Wiley & Sons Inc., 260 pp.
- Lécuyer C, Grandjean P and Sheppard SMF (1999) Oxygen isotope exchange between dissolved phosphate and water at temperatures $\leq 135^\circ\text{C}$: Inorganic versus biological fractionations. *Geochimica et Cosmochimica Acta* 63(6): 855–862.
- Lécuyer C, Amiot R, Touzeau A et al. (2013) Calibration of the phosphate $\delta^{18}\text{O}$ thermometer with carbonate-water oxygen isotope fractionation equations. *Chemical Geology* 347: 217–226.
- Lécuyer C, Fourel F, Martineau F et al. (2007) High-precision determination of $^{18}\text{O}/^{16}\text{O}$ ratios of silver phosphate by EA-pyrolysis-IRMS continuous flow technique. *Journal of Mass Spectrometry* 42: 36–41.
- Lécuyer C, Grandjean P, O'Neil JR et al. (1993) Thermal excursions in the ocean at the Cretaceous-Tertiary boundary (northern Morocco): $\delta^{18}\text{O}$ record of phosphatic fish debris. *Palaeogeography, Palaeoclimatology, Palaeoecology* 105: 235–243.
- Lécuyer C, Lézine AM, Fourel F et al. (2016) I-n-Atei paleolake documents past environmental changes in central Sahara at the time of the 'Green Sahara': Charcoal, carbon isotope and diatom records. *Palaeogeography, Palaeoclimatology, Palaeoecology* 441: 834–844.
- Legendre S (1986) Analysis of mammalian communities from the Late Eocene and Oligocene of southern France. *Palaeovertebrata* 16(4): 191–212.
- Levitus S, Burgett R and Boyer TP (1994) *World Ocean Atlas 1994* (Salinity: Technical Report, National Environmental Satellite, Data, and Information Service, vol. 3). Washington, DC: U.S. Government Printing Office.
- McCarroll D and Loader NJ (2004) Stable isotopes in tree rings. *Quaternary Science Reviews* 23: 771–801.
- McDermott F (2004) Palaeo-climate reconstruction from stable isotope variations in speleothems: A review. *Quaternary Science Reviews* 23: 901–918.
- Manning SW, Höflmayer F, Moeller N et al. (2014) Dating the Thera (Santorini) eruption: Archaeological and scientific evidence supporting a high chronology. *Antiquity* 88(342): 1164–1179.
- Matzarakis A and Nastos P (2011) Analysis of tourism potential for Crete Island, Greece. *Global NEST Journal* 13(2): 141–149.
- Novikova T, Papadopoulos GA and McCoy FW (2011) Modelling of tsunami generated by the giant Late Bronze Age eruption of Thera, South Aegean Sea, Greece. *Radiocarbon* 51(2): 397–411.
- O'Neil JR, Vennemann TW and McKenzie WF (2003) Effects of speciation on equilibrium fractionations and rates of oxygen isotope exchange between $(\text{PO}_4)_{\text{aq}}$ and H_2O . *Geochimica et Cosmochimica Acta* 67(17): 3135–3144.
- Pierre C (1999) The oxygen and carbon isotope distribution in the Mediterranean water masses. *Marine Geology* 153: 41–55.
- Román-Román P, Romero D and Torres-Ruiz F (2010) A diffusion process to model generalized von Bertalanffy growth patterns: Fitting to real data. *Journal of Theoretical Biology* 263: 59–69.
- Speer JH (2010) *Fundamentals of Tree Ring Research*. Tucson, AZ: The University of Arizona Press, 368 pp.
- Swart PK, Burns SJ and Leder JJ (1991) Fractionation of the stable isotopes of oxygen and carbon in carbon dioxide during the reaction of calcite with phosphoric acid as a function of temperature and technique. *Chemical Geology: Isotope Geo-science Section* 86: 89–96.
- Von Bertalanffy L (1938) A quantitative theory of organic growth. *Human Biology* 10(2): 181–213.
- Vrochidou AEK and Tsanis IK (2012) Assessing precipitation distribution impacts on droughts on the island of Crete. *Natural Hazards and Earth System Sciences* 12: 1159–1171.
- Ward SN (2002) Tsunamis. In: Meyers RA (ed.) *The Encyclopedia of Physical Science and Technology*, vol. 17. Amsterdam: Academic Press, pp. 175–191.
- Zazzo A, Lécuyer C and Mariotti A (2004) Experimentally-controlled carbon and oxygen isotope exchange between biapatites and water under inorganic and microbially-mediated conditions. *Geochimica et Cosmochimica Acta* 68(1): 1–12.
- Zazzo A, Mariotti A, Lécuyer C et al. (2002) Intra-tooth isotope variations in late Miocene bovid enamel from Afghanistan paleobiological, taphonomic, and climatic implications. *Palaeogeography, Palaeoclimatology, Palaeoecology* 186: 145–161.